1986AJ.....91.1301K

THE ASTRONOMICAL JOURNAL VOLUME 91, NUMBER 6 JUNE 1986

# DARK MATTER IN SPIRAL GALAXIES. I. GALAXIES WITH OPTICAL ROTATION CURVES

STEPHEN M. KENT[a)]
Harvard-Smithsonian Center for Astrophysics, 60 Garden Street, Cambridge, Massachusetts 02138

*Received 25 November 1985; revised 3 March 1986*

## ABSTRACT

Luminosity profiles measured with a CCD camera are presented for 37 Sb and Sc galaxies with existing optical rotation curves. A new method is developed for decomposing luminosity profiles into bulge and disk components. The mass distribution in these galaxies is modeled as the sum of bulge and disk components (with profiles given by the CCD data) and a dark halo. The rotation curves are used to determine the mass/light ratios of the bulge and disk components and two halo parameters. The observed rotation curves do not extend to a large enough radius to determine all parameters simultaneously. Three methods of constraining the halo or bulge/disk parameters are presented. At one extreme, the stellar mass/light ratio is set to the maximum value permitted by the rotation curve; in this case any additional halo component is quite modest in most galaxies. Most galaxies are also well fit by models with much more massive halos. However, it is argued that the former solution (modest halos) is probably closer to the truth. The resulting stellar mass/light ratio correlates with the mass, inclination, and morphological type of a galaxy.

## I. INTRODUCTION

In spiral galaxies, the presence of large amounts of unseen matter with a distribution different from that of the stars is now thought to be well established. The primary observational evidence for the existence of dark matter comes from optical and 21 cm rotation curves of spirals which do not show the expected Keplerian dropoff at large radii but remain flat or even rise over their entire observed range (Faber and Gallagher 1979; Bosma 1981; Rubin *et al.* 1985). On theoretical grounds, this dark matter is expected to be in the form of a spherical (halo) component in order to stabilize the spiral disks against bar instabilities (Ostriker and Peebles 1973). The nature of the dark matter is still unknown, although the current enthusiasm is for it to be some new fundamental particle. In current theories of galaxy formation, the existence of dark matter is quite important (White and Rees 1978; Faber 1982). Indeed, Faber predicts that the relative proportion of stellar to dark matter should increase along the Hubble sequence from elliptical to spiral galaxies.

To a certain extent, the fraction of mass in dark matter in a galaxy is indeterminate since the extent of the dark matter in any object is not well known (and galaxy halos may be sufficiently large that they overlap). Even within the domain where measurements exist, an actual measure of the fraction of dark matter has been made for only a handful of objects. In fact, Faber and Gallagher (1979) make an estimate of this fraction for various galaxy types, not from direct measurement but rather by comparing the global mass/light (M/L) ratio for each type with that expected from population-synthesis models.

One obstacle thus far to making a direct measurement has been the lack of good surface photometry for galaxies that have measured rotation curves and vice versa. With surface photometry it is possible to estimate the contribution to the rotation curve from the stellar component alone. Any excess in the observed rotation curve provides a measurement of the contribution of a dark component. The number of galaxies with a complete set of data is slowly growing [e.g., due to the work of Boroson (1981) and Wevers (1984)] and a joint analysis of dynamical and photometric data for a number of spiral galaxies has been made by Bosma and van der Kruit (1979), Kalnajs (1983), Casertano (1983), Carignan and Freeman (1985), and van Albada *et al.* (1985). This work suggests that the mass in dark matter is roughly the same as that in stars within a Holmberg radius, but whether this ratio is universal or depends on luminosity or morphological type is still not well known. Curiously, Kalnajs shows that the rotation curves for four galaxies which are flat or rising can be explained entirely in terms of a constant M/L ratio disk, suggesting that dark halos may not be as ubiquitous as is usually assumed. However, Van Albada *et al.* (1985) and Carignan and Freeman (1985) both point out that optical rotation curves seldom extend much past the expected peak in the rotation curve from the stellar disk and that 21 cm rotation curves which extend much farther leave little doubt as to the existence of "dark halos."

To increase the number of galaxies with both photometric and dynamical information, CCD images are being obtained for those galaxies with good existing rotation curves. In this paper, data are presented for 37 Sb and Sc galaxies with optical rotation curves measured by Rubin, Ford, and Thonnard (1980) and Rubin *et al.* (1982). Only a few of these galaxies have had previously measured photometry. The CCD images are used to derive luminosity profiles using standard reduction methods. For several galaxies, multicolor images have been obtained in order to investigate the effects of color gradients. A new method is presented for decomposing the profiles into bulge and disk components. If it is assumed that the M/L ratio is constant in the bulge and disk components, it is possible to compute the mass distribution and hence the rotation curve due to each component. By combining this information with the observed rotation curve, it should be possible to derive the distribution and mass of any dark halo. In practice, since the M/L ratio of the stellar component is not known *a priori*, it is necessary to make some assumptions about the halo mass distribution and estimate several parameters simultaneously. This has been done using three different assumptions about the halo density profile. A major result is that optical rotation curves usually do not place strong constraints on the amount of dark matter in these galaxies. Indeed, in agreement with Kalnajs (1983), some rotation curves are fit well without the need to assume the existence of *any* dark halo. Best estimates

---

[a)] Presidential Young Investigator and Alfred P. Sloan Fellow.

0004-6256/86/061301-27$00.90

of the stellar mass/light ratio will be derived, and various correlations explored.

## II. OBSERVATIONS AND REDUCTIONS

### *a) Sample*

The set of galaxies observed here consists of Sb and Sc galaxies with optical emission-line rotation curves measured by Rubin and collaborators. The revised curves tabulated by Rubin *et al.* (1985) will be used here. Of a total of 44 galaxies with rotation curves, photometry has been obtained for 37. Of the remainder, two are too large for the field of view of the CCD, three are too far south, and two lie close to nearby bright stars. The list of 37 galaxies along with other key information is given in Table I. Distances are computed directly from the redshifts assuming $H_0 = 50$.

### *b) Observations*

CCD images of the 37 galaxies were obtained using the Whipple Observatory 61 cm telescope on Mount Hopkins during the period 1983 November to 1984 April. The instrumentation and data-collection procedures were identical to those described by Kent (1983,1984) and will be summarized only here. The RCA CCD has a pixel format of 512 by 320 with a scale of 0.73" per pixel. Exposures were typically 20 min in the red *F* bandpass of Schild and Kent (1981). In addition, a few galaxies were also observed in *J* and *I* bandpasses. All observations were made under photometric or near-photometric conditions. Photometric calibration was accomplished by observing standard stars from the *uvgr* system of Thuan and Gunn (1976) and all magnitudes will be reduced to that system.

TABLE I. Spiral galaxies with optical rotation curves.

| Name<br>(1) | Type<br>(2) | Seeing FWHM (arcsec)<br>(3) | $\varepsilon_B$<br>(4) | $\varepsilon_D$<br>(5) | Pos. Ang.<br>(6) | B/T<br>(7) | D (Mpc)<br>(8) |
|---|---|---|---|---|---|---|---|
| I467 | Sc | 2.8 | - | 0.61 | 72 | - | 44.6 |
| N701 | Sc | 3.3 | - | 0.68 | 42 | - | 37.1 |
| N753 | Sc | 2.6 | 0.14 | 0.33 | 136 | 0.04 | 102.0 |
| N801 | Sc | 2.3 | 0.25 | 0.80 | 149 | 0.21 | 119.0 |
| N1035 | Sc | 2.8 | - | 0.72 | 147 | - | 24.7 |
| N1085 | Sb | 2.6 | 0.10 | 0.35 | 14: | 0.22 | 136.0 |
| N1087 | Sc | 2.1 | - | 0.36 | 0 | - | 30.8 |
| N1325 | Sb | 3.6 | 0.18 | 0.67 | 52 | 0.03 | 30.0 |
| N1353 | Sb | 2.7 | 0.26 | 0.60 | 137 | 0.15 | 30.0 |
| N1417 | Sb | 3.1 | 0.00 | 0.47 | 5 | 0.07 | 81.5 |
| N1421 | Sc | 3.0 | 0.27 | 0.79 | 179 | 0.05 | 40.0 |
| N1620 | Sb | 4.3 | 0.15 | 0.68 | 23 | 0.07 | 68.4 |
| N2590 | Sb | 2.5 | 0.46 | 0.71 | 77 | 0.25 | 95.8 |
| N2608 | Sc | 2.5 | 0.14 | 0.36 | 55: | 0.07 | 41.5 |
| N2708 | Sb | 3.0 | 0.00 | 0.60 | 20 | 0.08 | 35.5 |
| N2715 | Sc | 3.6 | 0.13 | 0.49 | 15: | 0.01 | 30.0 |
| N2742 | Sc | 2.9 | 0.11 | 0.47 | 86 | 0.01 | 27.6 |
| N2815 | Sb | 3.1 | 0.20 | 0.70 | 12 | 0.32 | 45.5 |
| N2998 | Sc | 2.1 | 0.19 | 0.51 | 58 | 0.02 | 95.6 |
| N3054 | Sb | 3.1 | 0.10 | 0.44 | 113 | 0.04 | 43.1 |
| N3067 | Sb | 2.3 | 0.38 | 0.60 | 102 | 0.03 | 28.3 |
| N3200 | Sb | 3.8 | 0.13 | 0.74 | 167 | 0.11 | 65.3 |
| N3495 | Sc | 2.7 | 0.37 | 0.79 | 20 | 0.02 | 19.4 |
| N4062 | Sc | 3.2 | 0.04 | 0.62 | 99 | 0.03 | 15.1 |
| N4448 | Sb | 3.0 | 0.10 | 0.65 | 92 | 0.22 | 19.0 |
| N4605 | Sc | 2.5 | - | 0.61 | 121 | 0.01 | 5.9 |
| N4682 | Sc | 3.5 | 0.23 | 0.50 | 82 | 0.02 | 43.4 |
| N4800 | Sb | 2.3 | 0.00 | 0.30 | 20: | 0.09 | 19.5 |
| N7171 | Sb | 3.3 | 0.28 | 0.56 | 119 | 0.04 | 57.4 |
| N7217 | Sb | 2.9 | 0.07 | 0.10 | 80: | 0.25 | 24.7 |
| N7537 | Sb | 2.9 | 0.30 | 0.72 | 76 | 0.18 | 57.3 |
| N7541 | Sc | 2.5 | 0.38 | 0.69 | 98 | 0.01 | 57.5 |
| N7606 | Sb | 3.3 | 0.40 | 0.59 | 147 | 0.08 | 47.5 |
| N7664 | Sc | 2.3 | 0.20 | 0.46 | 87 | 0.03 | 74.2 |
| U2885 | Sc | 2.6 | 0.12 | 0.58 | 45: | 0.14 | 118.0 |
| U11810 | Sb | 2.9 | 0.24 | 0.60 | 178 | 0.05 | 98.3 |
| U12810 | Sb | 3.0 | 0.17 | 0.62 | 54 | 0.07 | 165.0 |

### *c) Reductions*

Preliminary reductions are done using standardized procedures. The images are first debiased and flatfielded. Dark frames are scaled to the appropriate exposure time and subtracted. Blocked columns and other fixed defects are corrected by linear interpolation across the affected areas. Single-pixel cosmic-ray events are detected by an automatic algorithm and removed. The sky intensity is measured from a blank portion of the frame. The galaxies observed here are small enough that this is always possible. The seeing disk for each frame is determined by fitting a Gaussian profile to an isolated bright star.

### *d) Photometric Profiles*

The method for computing the luminosity profile of a galaxy is described by Kent (1983). Briefly, the isophotes of a galaxy are approximated by ellipses whose position angle and ellipticity are allowed to vary as a function of radius. At a given semimajor axis, the position angle and ellipticity are adjusted to make the $\sin 2E$ and $\cos 2E$ harmonics vanish along the ellipse. The intensity and shape parameters are then converted to major- and minor-axis profiles. Occasional checks show that the profiles determined in this way usually agree very well with single-line cuts through a galaxy but with a much improved signal/noise ratio. Disagreement is seen only in objects that show large isophote twists, but in such cases the position angle of the major and minor axes is not well defined. Such twists usually are due to the presence of bar components or strong spiral structure. However, since most of the present galaxies have high inclination, the presence of twists is seldom a problem.

For one galaxy, UGC 2885, a bright star clobbers the galaxy on one side. Consequently, the profile has been measured using a wedge-shaped cut along the major axis of the unperturbed side.

For reference, the mean position angle for an isophote at a surface brightness $\mu_r = 23$ is listed in Table I, column (6). Values marked with a colon (:) indicate the presence of significant isophote twisting. In most cases the agreement with Rubin, Ford, and Thonnard (1980) and Rubin *et al.* (1982) is excellent (better than 5°).

The complete list of major- and minor-axis profiles is given in Table II. The magnitudes have been converted to the *r* band of the *uvgr* system. A few profiles have been extrapolated by hand to match the range covered by the rotation curves. This extrapolation is done by fitting an exponential law to the outer part of the observed profile. For reference, a rough conversion to *B* magnitudes is $B = r + 1$. From photometry of Kent (1985), it is estimated that the Sun has an absolute magnitude in the *r* band of $M_r = 4.83$.

The photometric accuracy of the CCD profiles has been investigated extensively by Kent (1984). The major source of error is probably residual fluctuations in the sky background across the frame, which can produce systematic er-

TABLE II. Surface-brightness profiles.

| | IC467 | | N701 | | N753 | | N801 | | N1035 | | N1085 | | N1087 | | N1325 | |
|---|---|---|---|---|---|---|---|---|---|---|---|---|---|---|---|---|
| Radius Arcsec | Maj. Axis | Min. Axis | Maj. Axis | Min. Axis | Maj. Axis | Min. Axis | Maj. Axis | Min. Axis | Maj. Axis | Min. Axis | Maj. Axis | Min. Axis | Maj. Axis | Min. Axis | Maj. Axis | Min. Axis |
| 0.00 | 19.97 | 19.97 | 19.04 | 19.04 | 18.18 | 18.18 | 17.87 | 17.87 | 19.37 | 19.37 | 17.90 | 17.90 | 18.61 | 18.61 | 19.39 | 19.39 |
| 0.73 | 20.01 | 20.03 | 19.05 | 19.09 | 18.27 | 18.30 | 18.02 | 18.07 | 19.37 | 19.39 | 18.01 | 18.08 | 18.61 | 18.70 | 19.39 | 19.40 |
| 1.46 | 20.12 | 20.18 | 19.02 | 19.24 | 18.48 | 18.57 | 18.30 | 18.58 | 19.40 | 19.54 | 18.34 | 18.44 | 18.62 | 18.94 | 19.47 | 19.53 |
| 2.19 | 20.21 | 20.32 | 19.04 | 19.42 | 18.75 | 18.91 | 18.66 | 19.23 | 19.50 | 19.70 | 18.72 | 18.84 | 18.69 | 19.24 | 19.60 | 19.71 |
| 2.92 | 20.30 | 20.48 | 19.05 | 19.62 | 19.01 | 19.25 | 18.95 | 19.83 | 19.57 | 19.83 | 19.06 | 19.18 | 18.79 | 19.55 | 19.75 | 19.92 |
| 3.65 | 20.39 | 20.61 | 19.07 | 19.81 | 19.24 | 19.54 | 19.21 | 20.28 | 19.60 | 20.00 | 19.32 | 19.48 | 18.94 | 19.79 | 19.87 | 20.12 |
| 4.39 | 20.49 | 20.75 | 19.11 | 19.99 | 19.42 | 19.77 | 19.41 | 20.61 | 19.61 | 20.24 | 19.54 | 19.74 | 19.13 | 19.95 | 19.96 | 20.29 |
| 5.12 | 20.55 | 20.85 | 19.16 | 20.16 | 19.58 | 19.96 | 19.60 | 20.87 | 19.60 | 20.35 | 19.72 | 19.98 | 19.32 | 20.05 | 20.04 | 20.44 |
| 5.85 | 20.59 | 20.96 | 19.24 | 20.27 | 19.70 | 20.12 | 19.77 | 21.08 | 19.61 | 20.43 | 19.88 | 20.20 | 19.48 | 20.12 | 20.12 | 20.56 |
| 6.58 | 20.62 | 21.05 | 19.33 | 20.35 | 19.84 | 20.27 | 19.94 | 21.33 | 19.65 | 20.50 | 20.03 | 20.39 | 19.61 | 20.19 | 20.19 | 20.65 |
| 7.31 | 20.66 | 21.13 | 19.45 | 20.42 | 19.97 | 20.35 | 20.11 | 21.51 | 19.72 | 20.57 | 20.18 | 20.59 | 19.70 | 20.24 | 20.23 | 20.74 |
| 8.20 | 20.69 | 21.22 | 19.59 | 20.54 | 20.07 | 20.43 | 20.26 | 21.75 | 19.82 | 20.71 | 20.37 | 20.82 | 19.79 | 20.29 | 20.30 | 20.82 |
| 9.17 | 20.71 | 21.31 | 19.73 | 20.70 | 20.16 | 20.51 | 20.41 | 22.00 | 19.92 | 20.86 | 20.55 | 21.07 | 19.87 | 20.34 | 20.35 | 20.90 |
| 10.22 | 20.77 | 21.40 | 19.88 | 20.85 | 20.21 | 20.60 | 20.61 | 22.25 | 20.01 | 21.07 | 20.73 | 21.39 | 19.92 | 20.38 | 20.41 | 21.01 |
| 11.38 | 20.89 | 21.52 | 20.01 | 21.03 | 20.28 | 20.71 | 20.77 | 22.47 | 20.06 | 21.23 | 20.88 | 21.64 | 20.01 | 20.45 | 20.47 | 21.12 |
| 12.65 | 20.99 | 21.74 | 20.10 | 21.20 | 20.39 | 20.92 | 20.95 | 22.68 | 20.09 | 21.43 | 21.13 | 21.88 | 20.13 | 20.51 | 20.53 | 21.21 |
| 14.05 | 21.07 | 21.96 | 20.13 | 21.37 | 20.66 | 21.24 | 21.10 | 22.94 | 20.11 | 21.66 | 21.31 | 22.06 | 20.24 | 20.55 | 20.60 | 21.32 |
| 15.58 | 21.14 | 22.16 | 20.16 | 21.55 | 20.91 | 21.51 | 21.18 | 23.20 | 20.14 | 21.93 | 21.43 | 22.22 | 20.32 | 20.57 | 20.66 | 21.44 |
| 17.28 | 21.24 | 22.28 | 20.22 | 21.74 | 21.07 | 21.71 | 21.25 | 23.44 | 20.22 | 22.27 | 21.59 | 22.44 | 20.45 | 20.60 | 20.76 | 21.59 |
| 19.14 | 21.38 | 22.36 | 20.30 | 21.94 | 21.20 | 21.87 | 21.36 | 23.77 | 20.32 | 22.65 | 21.78 | 22.79 | 20.49 | 20.63 | 20.85 | 21.80 |
| 21.20 | 21.52 | 22.46 | 20.42 | 22.14 | 21.36 | 22.03 | 21.53 | 24.10 | 20.44 | 23.01 | 21.96 | 23.20 | 20.53 | 20.69 | 20.91 | 22.01 |
| 23.47 | 21.60 | 22.62 | 20.53 | 22.37 | 21.57 | 22.23 | 21.68 | 24.26 | 20.51 | 23.39 | 22.24 | 23.38 | 20.66 | 20.81 | 20.97 | 22.17 |
| 25.97 | 21.66 | 22.93 | 20.59 | 22.67 | 21.73 | 22.46 | 21.77 | | 20.57 | 23.76 | 22.64 | 23.62 | 20.83 | 20.96 | 21.01 | 22.36 |
| 28.74 | 21.63 | 23.47 | 20.73 | 23.01 | 21.92 | 22.69 | 21.89 | | 20.61 | 24.14 | 22.87 | 23.99 | 20.95 | 21.07 | 21.06 | 22.57 |
| 31.79 | 21.70 | 24.01 | 20.95 | 23.34 | 22.30 | 22.95 | 22.08 | | 20.69 | 24.60 | 23.07 | 24.20 | 21.03 | 21.26 | 21.11 | 22.83 |
| 35.16 | 21.78 | 24.62 | 21.15 | 23.63 | 22.52 | 23.21 | 22.19 | | 20.79 | 24.87 | 23.49 | 24.56 | 21.12 | 21.55 | 21.17 | 23.10 |
| 38.88 | 21.78 | 25.39 | 21.37 | 24.08 | 22.72 | 23.48 | 22.38 | | 20.95 | | 23.60 | 24.66 | 21.23 | 21.93 | 21.24 | 23.30 |
| 42.99 | 21.99 | 26.04 | 21.66 | 24.43 | 23.06 | 23.58 | 22.62 | | 21.09 | | 23.89 | 24.73 | 21.27 | 22.31 | 21.32 | |
| 47.53 | 22.30 | | 22.03 | 24.83 | 23.44 | 23.99 | 22.89 | | 21.39 | | 24.09 | 25.30 | 21.45 | 22.57 | 21.52 | |
| 52.55 | 22.61 | | 22.37 | 25.16 | 23.88 | 24.76 | 22.86 | | 21.80 | | 24.41 | 25.71 | 21.52 | 22.89 | 21.65 | |
| 58.09 | 22.85 | | 22.81 | | 23.92 | 25.44 | 22.89 | | 22.32 | | 24.85 | | 21.77 | 23.34 | 21.76 | |
| 64.22 | 22.98 | | 23.39 | | 23.98 | 25.84 | 23.07 | | 22.94 | | 25.01 | | 22.05 | 23.61 | 21.81 | |
| 70.98 | 23.22 | | 23.86 | | 24.62 | | 23.37 | | 23.66 | | | | 22.34 | | 22.02 | |
| 78.46 | 23.64 | | 24.45 | | 25.42 | | 23.57 | | 24.36 | | | | 22.61 | | 22.33 | |
| 86.72 | 24.37 | | | | | | 23.82 | | | | | | 22.95 | | 22.65 | |
| 95.85 | 25.75 | | | | | | 24.10 | | | | | | 23.33 | | 22.88 | |
| 105.94 | 26.50 | | | | | | | | | | | | | | 23.13 | |
| 117.09 | 27.25 | | | | | | | | | | | | | | | |

TABLE II. (continued)

| | N1353 | | N1417 | | N1421 | | N1620 | | N2590 | | N2608 | | N2708 | | N2715 | |
|---|---|---|---|---|---|---|---|---|---|---|---|---|---|---|---|---|
| Radius Arcsec | Maj. Axis | Min. Axis | Maj. Axis | Min. Axis | Maj. Axis | Min. Axis | Maj. Axis | Min. Axis | Maj. Axis | Min. Axis | Maj. Axis | Min. Axis | Maj. Axis | Min. Axis | Maj. Axis | Min. Axis |
| 0.00 | 17.41 | 17.41 | 17.65 | 17.65 | 18.91 | 18.91 | 19.17 | 19.17 | 18.35 | 18.35 | 17.96 | 17.96 | 18.01 | 18.01 | 19.56 | 19.56 |
| 0.73 | 17.50 | 17.57 | 17.75 | 17.75 | 18.96 | 18.98 | 19.18 | 19.21 | 18.39 | 18.52 | 18.14 | 18.19 | 18.07 | 18.09 | 19.57 | 19.59 |
| 1.46 | 17.72 | 17.95 | 18.01 | 18.04 | 19.08 | 19.16 | 19.26 | 19.30 | 18.54 | 18.92 | 18.52 | 18.66 | 18.25 | 18.26 | 19.62 | 19.67 |
| 2.19 | 18.04 | 18.42 | 18.35 | 18.40 | 19.24 | 19.39 | 19.37 | 19.45 | 18.73 | 19.28 | 19.02 | 19.24 | 18.45 | 18.52 | 19.73 | 19.79 |
| 2.92 | 18.37 | 18.82 | 18.67 | 18.77 | 19.41 | 19.63 | 19.50 | 19.67 | 18.88 | 19.57 | 19.42 | 19.69 | 18.65 | 18.82 | 19.86 | 19.93 |
| 3.65 | 18.69 | 19.09 | 18.95 | 19.13 | 19.55 | 19.82 | 19.62 | 19.90 | 19.04 | 19.78 | 19.73 | 19.99 | 18.83 | 19.09 | 19.98 | 20.09 |
| 4.39 | 18.97 | 19.31 | 19.16 | 19.43 | 19.68 | 19.96 | 19.73 | 20.13 | 19.22 | 20.03 | 19.94 | 20.19 | 19.00 | 19.33 | 20.08 | 20.22 |
| 5.12 | 19.20 | 19.49 | 19.33 | 19.71 | 19.80 | 20.06 | 19.83 | 20.32 | 19.40 | 20.36 | 20.10 | 20.35 | 19.12 | 19.55 | 20.18 | 20.33 |
| 5.85 | 19.33 | 19.62 | 19.47 | 19.98 | 19.90 | 20.13 | 19.91 | 20.50 | 19.59 | 20.67 | 20.22 | 20.47 | 19.24 | 19.74 | 20.27 | 20.42 |
| 6.58 | 19.43 | 19.72 | 19.60 | 20.19 | 19.97 | 20.24 | 19.99 | 20.63 | 19.79 | 21.01 | 20.33 | 20.56 | 19.35 | 19.92 | 20.34 | 20.49 |
| 7.31 | 19.52 | 19.79 | 19.69 | 20.36 | 20.04 | 20.25 | 20.06 | 20.74 | 19.95 | 21.19 | 20.39 | 20.67 | 19.43 | 20.10 | 20.41 | 20.55 |
| 8.20 | 19.61 | 19.87 | 19.80 | 20.53 | 20.07 | 20.29 | 20.15 | 20.85 | 20.11 | 21.33 | 20.48 | 20.75 | 19.54 | 20.32 | 20.49 | 20.59 |
| 9.17 | 19.71 | 19.93 | 19.90 | 20.68 | 20.12 | 20.38 | 20.25 | 20.96 | 20.24 | 21.49 | 20.57 | 20.84 | 19.65 | 20.56 | 20.55 | 20.63 |
| 10.22 | 19.81 | 20.00 | 20.00 | 20.81 | 20.14 | 20.53 | 20.34 | 21.05 | 20.34 | 21.71 | 20.64 | 21.09 | 19.76 | 20.81 | 20.61 | 20.70 |
| 11.38 | 19.91 | 20.12 | 20.12 | 20.94 | 20.14 | 20.66 | 20.42 | 21.14 | 20.43 | 21.96 | 20.75 | 21.18 | 19.86 | 21.04 | 20.65 | 20.75 |
| 12.65 | 19.99 | 20.28 | 20.24 | 21.09 | 20.12 | 20.84 | 20.51 | 21.23 | 20.53 | 22.24 | 20.88 | 21.32 | 19.98 | 21.29 | 20.68 | 20.80 |
| 14.05 | 20.07 | 20.52 | 20.38 | 21.19 | 20.13 | 21.12 | 20.58 | 21.37 | 20.71 | 22.52 | 20.93 | 21.41 | 20.10 | 21.47 | 20.69 | 20.89 |
| 15.58 | 20.16 | 20.77 | 20.58 | 21.30 | 20.15 | 21.41 | 20.66 | 21.55 | 20.85 | 22.88 | 20.88 | 21.53 | 20.21 | 21.62 | 20.71 | 20.98 |
| 17.28 | 20.26 | 20.96 | 20.80 | 21.45 | 20.20 | 21.71 | 20.75 | 21.78 | 20.91 | 23.38 | 20.82 | 21.64 | 20.34 | 21.79 | 20.75 | 21.05 |
| 19.14 | 20.35 | 21.14 | 20.93 | 21.69 | 20.29 | 21.98 | 20.81 | 22.09 | 20.99 | 24.12 | 20.89 | 21.75 | 20.46 | 22.01 | 20.78 | 21.15 |
| 21.20 | 20.49 | 21.32 | 20.98 | 22.14 | 20.34 | 22.32 | 20.86 | 22.41 | 21.12 | 24.69 | 20.99 | 21.91 | 20.60 | 22.25 | 20.88 | 21.28 |
| 23.47 | 20.51 | 21.56 | 21.05 | 22.42 | 20.38 | 22.62 | 20.92 | 22.66 | 21.18 | | 21.04 | 22.13 | 20.72 | 22.49 | 20.84 | 21.50 |
| 25.97 | 20.51 | 21.81 | 21.18 | 22.63 | 20.44 | 22.92 | 20.97 | 22.96 | 21.34 | | 21.14 | 22.40 | 20.86 | 22.72 | 20.86 | 21.69 |
| 28.74 | 20.50 | 22.12 | 21.33 | 22.81 | 20.59 | 23.20 | 21.07 | 23.31 | 21.49 | | 21.24 | 22.68 | 21.04 | 22.92 | 20.87 | 21.93 |
| 31.79 | 20.60 | 22.42 | 21.46 | 23.03 | 20.65 | 23.46 | 21.18 | 23.60 | 21.67 | | 21.29 | 22.93 | 21.20 | 23.20 | 20.92 | 22.22 |
| 35.16 | 20.66 | 22.79 | 21.65 | 23.32 | 20.73 | | 21.30 | | 21.89 | | 21.51 | 23.26 | 21.31 | 23.53 | 21.10 | 22.62 |
| 38.88 | 20.76 | 23.17 | 21.89 | 23.71 | 20.77 | | 21.43 | | 22.17 | | 21.70 | 23.52 | 21.45 | | 21.33 | 23.25 |
| 42.99 | 20.97 | 23.57 | 21.99 | 24.36 | 20.78 | | 21.61 | | 22.48 | | 22.03 | 23.70 | 21.71 | | 21.54 | |
| 47.53 | 21.33 | 23.83 | 22.04 | 24.56 | 20.76 | | 21.73 | | 22.89 | | 22.50 | 23.93 | 21.93 | | 21.72 | |
| 52.55 | 21.57 | | 22.15 | | 20.81 | | 21.85 | | 23.25 | | 23.06 | 24.27 | 22.12 | | 21.88 | |
| 58.09 | 21.76 | | 22.44 | | 20.87 | | 22.01 | | 23.39 | | 23.53 | | 22.36 | | 21.99 | |
| 64.22 | 21.90 | | 23.23 | | 21.04 | | 22.25 | | 23.77 | | 23.99 | | 22.69 | | 22.10 | |
| 70.98 | 22.04 | | 23.84 | | 21.01 | | 22.69 | | | | | | 23.07 | | 22.20 | |
| 78.46 | 22.40 | | 24.12 | | 21.22 | | 23.19 | | | | | | 23.41 | | 22.35 | |
| 86.72 | 22.86 | | | | 21.58 | | 23.50 | | | | | | | | 22.55 | |
| 95.85 | 23.31 | | | | 22.09 | | | | | | | | | | 22.67 | |
| 105.94 | | | | | 22.65 | | | | | | | | | | 22.85* | |
| 117.09 | | | | | 23.11 | | | | | | | | | | 23.05* | |
| 129.41 | | | | | | | | | | | | | | | 23.27* | |
| 143.03 | | | | | | | | | | | | | | | 23.52* | |

TABLE II. (continued)

| | N2742 | | N2815 | | N2998 | | N3054 | | N3067 | | N3200 | | N3495 | | N4062 | |
|---|---|---|---|---|---|---|---|---|---|---|---|---|---|---|---|---|
| Radius Arcsec | Maj. Axis | Min. Axis | Maj. Axis | Min. Axis | Maj. Axis | Min. Axis | Maj. Axis | Min. Axis | Maj. Axis | Min. Axis | Maj. Axis | Min. Axis | Maj. Axis | Min. Axis | Maj. Axis | Min. Axis |
| 0.00 | 19.23 | 19.23 | 18.13 | 18.13 | 18.81 | 18.81 | 17.81 | 17.81 | 18.59 | 18.59 | 18.19 | 18.19 | 19.95 | 19.95 | 19.05 | 19.05 |
| 0.73 | 19.29 | 19.29 | 18.18 | 18.21 | 18.94 | 18.99 | 17.89 | 17.91 | 18.64 | 18.71 | 18.22 | 18.25 | 19.96 | 20.01 | 19.08 | 19.09 |
| 1.46 | 19.40 | 19.45 | 18.32 | 18.39 | 19.19 | 19.33 | 18.11 | 18.18 | 18.75 | 18.95 | 18.36 | 18.43 | 20.02 | 20.11 | 19.16 | 19.20 |
| 2.19 | 19.56 | 19.66 | 18.50 | 18.62 | 19.46 | 19.69 | 18.41 | 18.54 | 18.92 | 19.21 | 18.57 | 18.68 | 20.11 | 20.26 | 19.27 | 19.34 |
| 2.92 | 19.71 | 19.87 | 18.68 | 18.83 | 19.67 | 19.95 | 18.70 | 18.93 | 19.05 | 19.43 | 18.82 | 18.98 | 20.19 | 20.43 | 19.38 | 19.50 |
| 3.65 | 19.83 | 20.07 | 18.86 | 19.01 | 19.81 | 20.13 | 18.97 | 19.29 | 19.18 | 19.57 | 19.09 | 19.32 | 20.29 | 20.60 | 19.49 | 19.64 |
| 4.39 | 19.94 | 20.20 | 19.01 | 19.18 | 19.91 | 20.26 | 19.19 | 19.61 | 19.29 | 19.67 | 19.37 | 19.64 | 20.39 | 20.73 | 19.59 | 19.77 |
| 5.12 | 20.04 | 20.30 | 19.12 | 19.33 | 19.98 | 20.42 | 19.38 | 19.87 | 19.39 | 19.78 | 19.62 | 19.94 | 20.47 | 20.84 | 19.67 | 19.89 |
| 5.85 | 20.13 | 20.38 | 19.23 | 19.47 | 20.02 | 20.55 | 19.54 | 20.11 | 19.46 | 19.99 | 19.84 | 20.22 | 20.54 | 20.95 | 19.75 | 20.00 |
| 6.58 | 20.22 | 20.46 | 19.32 | 19.60 | 20.08 | 20.62 | 19.67 | 20.29 | 19.52 | 20.09 | 20.04 | 20.45 | 20.60 | 21.04 | 19.81 | 20.10 |
| 7.31 | 20.27 | 20.54 | 19.41 | 19.70 | 20.13 | 20.69 | 19.78 | 20.43 | 19.59 | 20.15 | 20.20 | 20.68 | 20.66 | 21.21 | 19.87 | 20.18 |
| 8.20 | 20.34 | 20.61 | 19.52 | 19.82 | 20.20 | 20.79 | 19.90 | 20.55 | 19.66 | 20.25 | 20.36 | 20.94 | 20.73 | 21.26 | 19.92 | 20.26 |
| 9.17 | 20.40 | 20.68 | 19.65 | 19.91 | 20.26 | 20.92 | 20.00 | 20.64 | 19.71 | 20.39 | 20.49 | 21.12 | 20.81 | 21.32 | 19.98 | 20.33 |
| 10.22 | 20.45 | 20.72 | 19.78 | 20.03 | 20.32 | 21.12 | 20.10 | 20.71 | 19.76 | 20.60 | 20.60 | 21.29 | 20.87 | 21.40 | 20.05 | 20.38 |
| 11.38 | 20.47 | 20.76 | 19.93 | 20.19 | 20.40 | 21.48 | 20.19 | 20.79 | 19.78 | 20.80 | 20.68 | 21.41 | 20.93 | 21.53 | 20.11 | 20.44 |
| 12.65 | 20.51 | 20.78 | 20.08 | 20.42 | 20.61 | 21.62 | 20.28 | 20.87 | 19.81 | 20.96 | 20.74 | 21.57 | 20.98 | 21.68 | 20.17 | 20.51 |
| 14.05 | 20.56 | 20.84 | 20.23 | 20.67 | 20.95 | 21.78 | 20.39 | 21.09 | 19.83 | 21.21 | 20.78 | 21.75 | 21.04 | 21.76 | 20.23 | 20.62 |
| 15.58 | 20.61 | 20.93 | 20.39 | 20.95 | 21.13 | 21.91 | 20.49 | 21.30 | 19.86 | 21.56 | 20.82 | 21.96 | 21.07 | 21.84 | 20.28 | 20.81 |
| 17.28 | 20.65 | 21.01 | 20.55 | 21.34 | 21.19 | 22.06 | 20.60 | 21.40 | 19.97 | 21.94 | 20.87 | 22.20 | 21.09 | 21.95 | 20.32 | 20.98 |
| 19.14 | 20.68 | 21.09 | 20.71 | 21.73 | 21.22 | 22.30 | 20.73 | 21.46 | 20.20 | 22.40 | 20.90 | 22.37 | 21.09 | 22.10 | 20.37 | 21.08 |
| 21.20 | 20.70 | 21.21 | 20.85 | 22.02 | 21.27 | 22.69 | 20.83 | 21.53 | 20.46 | 22.82 | 20.95 | 22.58 | 21.12 | 22.28 | 20.44 | 21.17 |
| 23.47 | 20.69 | 21.33 | 20.97 | 22.36 | 21.33 | 23.13 | 20.93 | 21.56 | 20.60 | 23.20 | 20.99 | 22.88 | 21.13 | 22.50 | 20.52 | 21.29 |
| 25.97 | 20.71 | 21.48 | 21.10 | 22.84 | 21.48 | 23.35 | 21.00 | 21.63 | 20.72 | 23.61 | 21.05 | 23.31 | 21.14 | 22.89 | 20.62 | 21.48 |
| 28.74 | 20.78 | 21.74 | 21.22 | 23.25 | 21.91 | 23.71 | 21.06 | 21.82 | 20.89 | 24.06 | 21.12 | | 21.14 | | 20.70 | 21.72 |
| 31.79 | 20.84 | 22.00 | 21.30 | 23.65 | 22.13 | 23.96 | 21.12 | 22.12 | 21.11 | 24.38 | 21.18 | | 21.16 | | 20.75 | 21.99 |
| 35.16 | 20.89 | 22.28 | 21.36 | 23.93 | 22.28 | 24.27 | 21.20 | 22.30 | 21.29 | 24.66 | 21.22 | | 21.15 | | 20.80 | 22.23 |
| 38.88 | 21.03 | 22.65 | 21.45 | | 22.42 | 24.53 | 21.36 | 22.50 | 21.42 | 25.08 | 21.36 | | 21.18 | | 20.83 | 22.51 |
| 42.99 | 21.29 | 23.07 | 21.60 | | 22.58 | 24.89 | 21.59 | 22.76 | 21.59 | 25.58 | 21.57 | | 21.26 | | 20.83 | 22.83 |
| 47.53 | 21.52 | 23.45 | 21.81 | | 22.92 | | 21.79 | 23.05 | 21.83 | | 21.76 | | 21.38 | | 20.82 | 23.28 |
| 52.55 | 21.63 | 23.83 | 21.99 | | 23.49 | | 21.89 | 23.30 | 22.07 | | 21.88 | | 21.46 | | 20.92 | 23.72 |
| 58.09 | 21.78 | 24.05 | 22.17 | | 23.67 | | 21.98 | 23.56 | 22.35 | | 21.96 | | 21.44 | | 21.16 | |
| 64.22 | 21.95 | | 22.30 | | 24.02 | | 22.32 | 24.13 | 23.08 | | 22.02 | | 21.49 | | 21.45 | |
| 70.98 | 22.18 | | 22.40 | | 24.24 | | 22.73 | 24.79 | 24.14 | | 22.25 | | 21.62 | | 21.69 | |
| 78.46 | 22.73 | | 22.51 | | 24.55 | | 23.08 | | | | 22.77 | | 21.90 | | 21.84 | |
| 86.72 | 23.40 | | 22.72 | | | | 23.42 | | | | 23.09 | | 22.06 | | 22.09 | |
| 95.85 | 23.99 | | 23.25 | | | | 23.62 | | | | 23.29 | | 22.31 | | 22.40 | |
| 105.94 | | | | | | | 24.11 | | | | 23.52 | | 22.71 | | 22.79 | |
| 117.09 | | | | | | | 25.09 | | | | 23.78 | | 23.06 | | 23.26 | |
| 129.41 | | | | | | | 26.13 | | | | 24.06 | | 23.54 | | 23.77 | |
| 143.03 | | | | | | | | | | | 24.37 | | 24.13 | | 24.33 | |

TABLE II. (continued)

| Radius Arcsec | N4448 Maj. Axis | N4448 Min. Axis | N4605 Maj. Axis | N4605 Min. Axis | N4682 Maj. Axis | N4682 Min. Axis | N4800 Maj. Axis | N4800 Min. Axis | N7171 Maj. Axis | N7171 Min. Axis | N7217 Maj. Axis | N7217 Min. Axis | N7537 Maj. Axis | N7537 Min. Axis | N7541 Maj. Axis | N7541 Min. Axis |
|---|---|---|---|---|---|---|---|---|---|---|---|---|---|---|---|---|
| 0.00 | 17.59 | 17.59 | 18.64 | 18.64 | 19.98 | 19.98 | 17.07 | 17.07 | 19.18 | 19.18 | 16.74 | 16.74 | 18.77 | 18.77 | 18.94 | 18.94 |
| 0.73 | 17.63 | 17.65 | 18.73 | 18.74 | 20.00 | 20.04 | 17.19 | 17.19 | 19.22 | 19.27 | 16.82 | 16.83 | 18.81 | 18.85 | 18.98 | 19.03 |
| 1.46 | 17.72 | 17.80 | 18.95 | 19.00 | 20.10 | 20.18 | 17.44 | 17.48 | 19.33 | 19.48 | 17.01 | 17.03 | 18.92 | 19.06 | 19.05 | 19.25 |
| 2.19 | 17.87 | 17.99 | 19.14 | 19.22 | 20.22 | 20.36 | 17.80 | 17.85 | 19.52 | 19.74 | 17.25 | 17.29 | 19.07 | 19.32 | 19.15 | 19.47 |
| 2.92 | 18.02 | 18.19 | 19.25 | 19.36 | 20.36 | 20.52 | 18.14 | 18.19 | 19.70 | 20.00 | 17.50 | 17.52 | 19.20 | 19.60 | 19.23 | 19.64 |
| 3.65 | 18.16 | 18.37 | 19.29 | 19.39 | 20.49 | 20.65 | 18.39 | 18.46 | 19.85 | 20.21 | 17.70 | 17.72 | 19.32 | 19.88 | 19.32 | 19.79 |
| 4.39 | 18.30 | 18.54 | 19.31 | 19.40 | 20.58 | 20.75 | 18.56 | 18.66 | 19.97 | 20.40 | 17.87 | 17.90 | 19.40 | 20.18 | 19.42 | 19.91 |
| 5.12 | 18.44 | 18.69 | 19.34 | 19.42 | 20.64 | 20.84 | 18.69 | 18.81 | 20.11 | 20.57 | 18.02 | 18.05 | 19.47 | 20.49 | 19.50 | 20.04 |
| 5.85 | 18.58 | 18.81 | 19.39 | 19.46 | 20.69 | 20.95 | 18.82 | 18.95 | 20.22 | 20.71 | 18.14 | 18.20 | 19.54 | 20.79 | 19.57 | 20.06 |
| 6.58 | 18.71 | 18.92 | 19.40 | 19.51 | 20.74 | 21.04 | 18.92 | 19.09 | 20.32 | 20.82 | 18.27 | 18.35 | 19.63 | 21.06 | 19.63 | 20.09 |
| 7.31 | 18.84 | 19.02 | 19.41 | 19.56 | 20.77 | 21.10 | 19.01 | 19.22 | 20.40 | 20.93 | 18.40 | 18.48 | 19.72 | 21.33 | 19.68 | 20.11 |
| 8.20 | 18.99 | 19.13 | 19.39 | 19.67 | 20.85 | 21.17 | 19.11 | 19.37 | 20.49 | 21.05 | 18.54 | 18.61 | 19.88 | 21.64 | 19.74 | 20.21 |
| 9.17 | 19.14 | 19.27 | 19.40 | 19.74 | 20.92 | 21.25 | 19.20 | 19.55 | 20.58 | 21.12 | 18.68 | 18.75 | 20.04 | 21.92 | 19.78 | 20.44 |
| 10.22 | 19.29 | 19.43 | 19.43 | 19.81 | 20.98 | 21.33 | 19.30 | 19.76 | 20.67 | 21.14 | 18.80 | 18.90 | 20.22 | 22.21 | 19.82 | 20.60 |
| 11.38 | 19.44 | 19.60 | 19.48 | 19.93 | 21.02 | 21.40 | 19.43 | 19.97 | 20.74 | 21.17 | 18.93 | 19.04 | 20.38 | 22.58 | 19.88 | 20.74 |
| 12.65 | 19.60 | 19.77 | 19.56 | 20.04 | 21.07 | 21.46 | 19.55 | 20.19 | 20.80 | 21.24 | 19.08 | 19.18 | 20.53 | 23.05 | 19.93 | 20.87 |
| 14.05 | 19.76 | 19.96 | 19.61 | 20.21 | 21.10 | 21.54 | 19.71 | 20.38 | 20.86 | 21.32 | 19.23 | 19.32 | 20.69 | 23.50 | 19.97 | 21.04 |
| 15.58 | 19.92 | 20.20 | 19.59 | 20.35 | 21.14 | 21.67 | 19.90 | 20.59 | 20.92 | 21.40 | 19.38 | 19.46 | 20.87 | 23.85 | 19.97 | 21.27 |
| 17.28 | 20.05 | 20.58 | 19.61 | 20.47 | 21.20 | 21.89 | 20.07 | 20.80 | 20.99 | 21.58 | 19.51 | 19.60 | 21.09 | 24.22 | 19.99 | 21.53 |
| 19.14 | 20.17 | 20.94 | 19.72 | 20.59 | 21.26 | 22.06 | 20.21 | 20.97 | 21.04 | 21.92 | 19.65 | 19.75 | 21.31 | 24.63 | 20.06 | 21.76 |
| 21.20 | 20.28 | 21.19 | 19.82 | 20.75 | 21.29 | 22.21 | 20.32 | 21.14 | 21.12 | 22.13 | 19.79 | 19.88 | 21.49 | 24.86 | 20.19 | 22.03 |
| 23.47 | 20.37 | 21.47 | 19.84 | 20.93 | 21.31 | 22.46 | 20.49 | 21.36 | 21.24 | 22.26 | 19.92 | 20.01 | 21.63 | 25.25 | 20.23 | 22.33 |
| 25.97 | 20.43 | 21.85 | 19.79 | 21.12 | 21.42 | 22.74 | 20.70 | 21.57 | 21.46 | 22.42 | 20.04 | 20.15 | 21.75 |  | 20.22 | 22.60 |
| 28.74 | 20.46 | 22.23 | 19.81 | 21.31 | 21.61 | 23.00 | 20.90 | 21.74 | 21.54 | 22.60 | 20.15 | 20.32 | 21.94 |  | 20.37 | 22.96 |
| 31.79 | 20.51 | 22.57 | 19.87 | 21.54 | 21.70 | 23.32 | 21.11 | 22.01 | 21.61 | 22.96 | 20.29 | 20.49 | 22.17 |  | 20.36 | 23.41 |
| 35.16 | 20.57 | 22.92 | 19.78 | 21.80 | 21.78 | 23.74 | 21.44 | 22.45 | 21.71 | 23.59 | 20.47 | 20.67 | 22.38 |  | 20.39 | 23.92 |
| 38.88 | 20.64 | 23.26 | 19.83 | 22.02 | 21.90 | 24.24 | 21.82 | 22.95 | 21.85 | 24.37 | 20.68 | 20.89 | 22.63 |  | 20.62 | 24.40 |
| 42.99 | 20.73 | 23.61 | 20.01 | 22.27 | 22.10 | 24.76 | 22.20 | 23.34 | 22.02 |  | 20.88 | 21.08 | 22.89 |  | 20.87 | 24.77 |
| 47.53 | 20.90 | 23.96 | 20.10 | 22.53 | 22.36 |  | 22.67 | 23.67 | 22.23 |  | 21.09 | 21.28 | 23.19 |  | 21.12 |  |
| 52.55 | 21.14 | 24.32 | 20.16 | 22.80 | 22.68 |  | 23.17 | 23.97 | 22.61 |  | 21.29 | 21.47 | 23.64 |  | 21.24 |  |
| 58.09 | 21.32 |  | 20.25 | 23.07 | 23.08 |  | 23.67 | 24.21 | 23.12 |  | 21.52 | 21.66 | 24.17 |  | 21.42 |  |
| 64.22 | 21.45 |  | 20.41 | 23.36 | 23.41 |  | 24.03 | 24.49 | 23.65 |  | 21.70 | 21.78 | 24.84 |  | 21.76 |  |
| 70.98 | 21.54 |  | 20.70 | 23.58 | 23.77 |  | 24.26 | 24.74 |  |  | 21.84 | 22.05 |  |  | 22.20 |  |
| 78.46 | 21.74 |  | 21.12 |  | 24.31 |  | 24.52 |  |  |  | 22.06 | 22.49 |  |  | 22.69 |  |
| 86.72 | 22.18 |  | 21.55 |  |  |  |  |  |  |  | 22.32 | 22.86 |  |  | 23.24 |  |
| 95.85 | 22.66 |  | 21.79 |  |  |  |  |  |  |  | 22.80 | 23.14 |  |  | 24.22 |  |
| 105.94 | 23.24 |  | 22.18 |  |  |  |  |  |  |  | 23.23 | 23.44 |  |  |  |  |
| 117.09 | 23.86 |  | 22.62 |  |  |  |  |  |  |  |  |  |  |  |  |  |
| 129.41 |  |  | 22.98 |  |  |  |  |  |  |  |  |  |  |  |  |  |
| 143.03 |  |  | 23.28 |  |  |  |  |  |  |  |  |  |  |  |  |  |

1986AJ.....91.1301K

TABLE II. (continued)

| Radius Arcsec | N7606 | | N7664 | | U2885 | | U11810 | | U12810 | |
|---|---|---|---|---|---|---|---|---|---|---|
| | Maj. Axis | Min. Axis | Maj. Axis | Min. Axis | Maj. Axis | Min. Axis | Maj. Axis | Min. Axis | Maj. Axis | Min. Axis |
| 0.00 | 17.73 | 17.73 | 18.10 | 18.10 | 18.40 | | 19.55 | 19.55 | 19.29 | 19.29 |
| 0.73 | 17.80 | 17.82 | 18.19 | 18.31 | 18.52 | | 19.63 | 19.70 | 19.36 | 19.38 |
| 1.46 | 17.97 | 18.04 | 18.39 | 18.71 | 18.83 | | 19.82 | 19.96 | 19.60 | 19.67 |
| 2.19 | 18.20 | 18.34 | 18.64 | 19.09 | 19.21 | | 20.00 | 20.30 | 19.93 | 20.04 |
| 2.92 | 18.43 | 18.66 | 18.89 | 19.36 | 19.54 | | 20.21 | 20.66 | 20.24 | 20.42 |
| 3.65 | 18.64 | 18.96 | 19.10 | 19.58 | 19.85 | | 20.39 | 20.94 | 20.48 | 20.80 |
| 4.39 | 18.83 | 19.23 | 19.28 | 19.77 | 20.09 | | 20.53 | 21.12 | 20.63 | 21.08 |
| 5.12 | 18.99 | 19.45 | 19.42 | 19.93 | 20.36 | | 20.67 | 21.34 | 20.73 | 21.27 |
| 5.85 | 19.12 | 19.65 | 19.53 | 20.10 | 20.58 | | 20.78 | 21.48 | 20.80 | 21.36 |
| 6.58 | 19.25 | 19.82 | 19.64 | 20.23 | 20.77 | | 20.87 | 21.59 | 20.84 | 21.46 |
| 7.31 | 19.36 | 19.95 | 19.72 | 20.34 | 20.93 | | 20.98 | 21.71 | 20.86 | 21.55 |
| 8.20 | 19.47 | 20.07 | 19.82 | 20.52 | 21.04 | | 21.11 | 21.83 | 20.92 | 21.74 |
| 9.17 | 19.59 | 20.18 | 19.93 | 20.77 | 21.17 | | 21.20 | 22.03 | 20.97 | 21.91 |
| 10.22 | 19.71 | 20.28 | 20.07 | 21.12 | 21.24 | | 21.26 | 22.29 | 21.02 | 22.07 |
| 11.38 | 19.81 | 20.39 | 20.10 | 21.36 | 21.31 | | 21.27 | 22.79 | 21.09 | 22.23 |
| 12.65 | 19.91 | 20.47 | 20.21 | 21.59 | 21.37 | | 21.39 | 23.01 | 21.09 | 22.39 |
| 14.05 | 20.00 | 20.59 | 20.38 | 21.86 | 21.45 | | 21.52 | 23.21 | 21.10 | 22.57 |
| 15.58 | 20.08 | 20.70 | 20.61 | 22.17 | 21.55 | | 21.59 | 23.45 | 21.18 | 22.83 |
| 17.28 | 20.14 | 20.77 | 20.84 | 22.55 | 21.60 | | 21.61 | 23.74 | 21.32 | 23.29 |
| 19.14 | 20.20 | 20.84 | 20.95 | 22.95 | 21.71 | | 21.71 | 24.15 | 21.44 | 23.91 |
| 21.20 | 20.25 | 20.91 | 21.18 | 23.19 | 21.86 | | 21.97 | 24.83 | 21.57 | 24.54 |
| 23.47 | 20.29 | 20.99 | 21.55 | 23.56 | 21.92 | | 22.19 | | 21.73 | |
| 25.97 | 20.31 | 21.21 | 21.96 | 23.81 | 22.00 | | 22.38 | | 22.05 | |
| 28.74 | 20.36 | 21.45 | 22.31 | 24.11 | 22.01 | | 22.50 | | 22.50 | |
| 31.79 | 20.47 | 21.69 | 22.56 | 24.34 | 21.99 | | 22.65 | | 22.76 | |
| 35.16 | 20.55 | 21.87 | 22.86 | 24.66 | 22.04 | | 22.70 | | 22.93 | |
| 38.88 | 20.61 | 22.12 | 23.29 | 25.12 | 22.10 | | 22.78 | | 23.10 | |
| 42.99 | 20.78 | 22.56 | 23.88 | | 22.05 | | 23.17 | | 23.33 | |
| 47.53 | 21.01 | 23.04 | 24.09 | | 22.10 | | 23.79 | | 23.57 | |
| 52.55 | 21.03 | 23.61 | 24.30 | | 22.36 | | 24.36 | | 24.13 | |
| 58.09 | 21.12 | | 24.59 | | 22.53 | | | | | |
| 64.22 | 21.38 | | 24.90 | | 22.75 | | | | | |
| 70.98 | 21.62 | | 25.23 | | 22.96 | | | | | |
| 78.46 | 21.76 | | 25.59* | | 23.09 | | | | | |
| 86.72 | 21.96 | | 25.99* | | 23.55 | | | | | |
| 95.85 | 22.24 | | 26.44* | | 24.07 | | | | | |
| 105.94 | 22.43 | | | | 24.55 | | | | | |
| 117.09 | 22.77 | | | | 25.01 | | | | | |
| 129.41 | 23.37 | | | | 25.53 | | | | | |
| 143.03 | 23.97* | | | | 26.12 | | | | | |

*Profile extended by hand

rors of 0.2 mag at a surface brightness of $\mu_r = 24$. A comparison of images of the same galaxy from different observing seasons occasionally does show such discrepancies.

## III. COLOR GRADIENTS

One of the assumptions that will be made later is that the mass/light ratio is constant within the bulge and disk components of a galaxy. A check that can be made on this assumption is to look at color gradients. A necessary (although not sufficient) condition for the M/L ratio to be constant is that the color within each component likewise be constant (stellar population differences between the bulge and disk may still produce a gradient in the total galaxy color profile).

Thirteen galaxies have three-color photometry in the *J*, *F*, and *I* bands (the *J* band lies at 4700 Å, roughly halfway between the standard *B* and *V* bands, while the *I* band is centered at 8600 Å). The $J-I$ color gradients of these galaxies are plotted as a function of the *r* surface brightness in Fig. 1. Note that these plots refer to the local, not cumulative, colors. The color zero point for the combined set of galaxies is arbitrary. In a couple of cases, differences in seeing between the different frames cause spurious gradients at high surface brightness. Systematic errors in the sky subtraction make the colors unreliable for $\mu_r > 24$. This figure shows the following results:

(1) The gradients away from the center are primarily in the sense of red to blue.

(2) The largest gradient in $J-I$ is 1 mag for NGC 753; most objects have much smaller gradients. The range of color spanned by NGC 753 alone nearly covers the entire range of color among all galaxies. The slope of the gradient $d(J-I)/dF$ seldom exceeds 10%.

(3) From examining $J-F$ and $F-I$ separately, the bulk of the gradient is due to differences between the *J* and *F* bands.

(4) The intrinsically large galaxies (NGC 753 and NGC 801) have significant red-to-blue gradients. The smallest galaxy, NGC 4605, is the only object with a substantial blue-to-red gradient away from the center. The remaining galaxies have gradients that are small or negligible (with the exception of NGC 3067).

(5) An examination of the individual *J*, *F*, and *I* profiles shows that the *I* profiles are the smoothest, as would be expected if local bumps in profiles are due to regions of star formation. Overall, however, the profiles in different colors follow one another closely.

(6) One notable feature in the gradient profiles is the occurrence of distinct steps where the color suddenly jumps blueward. These steps correspond to plateaus in the luminosity profile. Some of these steps can be correlated with regions where the profiles pass from bulge dominated to disk dominated. However, such steps are not always seen, nor are they always correlated with a bulge-disk transition.

Similar work on color gradients has been done by Elmegreen and Elmegreen (1984,1985), who measured the profiles of many spirals in *B* and *I* bandpasses. From an examination of the figures in these two papers, one finds that several of their galaxies have much steeper gradients than found here (the worst case being NGC 5055, which has a slope approaching 50%). Unfortunately, none of their galaxies overlap those observed here. If the Elmegreens' profiles are correct, however, the assumption of constant mass/light ratio would have to be discarded or at least checked for each galaxy on an individual basis.

## IV. PROFILE DECOMPOSITION

To a first approximation, a spiral galaxy can be decomposed into a spheroidal bulge component and a flat disk component. For the computation of rotation curves, it is important to know the distribution of light in each component since they contribute in different ways. Most commonly, the decomposition is done by parametrizing each component with some density law that has scale parameters that are determined by fitting the laws to the observed profile of the galaxy. The laws most widely used are a de Vaucouleurs $r^{1/4}$ law profile (de Vaucouleurs 1948) for the bulge and an exponential profile for the disk.

While this method has been used extensively in the past, it suffers from the problem that many galaxies are not described well by the two fitting laws. This problem manifests itself in two ways. First, disks are seldom well represented by a single exponential law over their entire range. Significant structure is introduced by spiral arms, lenses, and rings (bars are also a problem but were avoided deliberately by Rubin *et al.*). Disks also can have global shapes that fall off less steeply or more steeply than exponential. Second, the bulges probably fall off more steeply than an $r^{1/4}$ law in regions where the disk dominates. Often, the formal decomposition of a late-type galaxy into bulge and disk components produces a bulge that contributes significant light in a region where a visual inspection would suggest the disk ought to dominate. Occasionally, the fit of an $r^{1/4}$ law to the central bulge predicts more light from the bulge alone at large radii than is actually observed in the entire galaxy.

For these reasons, it was decided to use an alternative method of profile decomposition which does not depend on the use of *a priori* fitting laws. It is assumed that the bulge and disk each have luminosity profiles that, in projection, have elliptical isophotes of constant flattening. This would be true, for example, if the bulge were an oblate spheroid and the disk were axisymmetric and infinitely thin. Then the galaxy major- and minor-axis profiles are each the sum of the two individual luminosity profiles of the bulge and disk but with different radial scale factors. If the apparent flattening of the bulge and disk are different, then the major- and minor-axis profiles can be decomposed uniquely to recover the individual profiles. The method is implemented as follows. Let $\mu_{\rm B}(r)$ and $\mu_{\rm D}(r)$ be the apparent major-axis surface-brightness profiles of the bulge and disk, respectively. Let $f_{\rm B}$ and $f_{\rm D}$ be the major/minor axis ratio of each component $(=a/b=1/[1-\epsilon])$. Then the major-axis profile $p(r)$ and minor-axis profile $q(r)$ are given by

$$p(r)=\mu_{\rm B}(r)+\mu_{\rm D}(r)\,, \qquad (1)$$

$$q(r)=\mu_{\rm B}(f_{\rm B}r)+\mu_{\rm D}(f_{\rm D}r)\,.$$

Define $w(r)$ as

$$w(r)=q(r)-p(f_{\rm D}r)\,.$$

Then

$$\mu_{\rm B}(r)=w(r/f_{\rm B})-\mu_{\rm B}(f_{\rm D}r/f_{\rm B})\,. \qquad (2)$$

Provided $f_{\rm D} > f_{\rm B}$, this equation can be used to determine the bulge profile iteratively. The function $w(r)$ is known from the observed major- and minor-axis profiles. In the first iteration, $\mu_{\rm B}$ is set equal to $w$. It is then substituted into the right-hand side of Eq. (2) and a new $\mu_{\rm B}$ computed. The

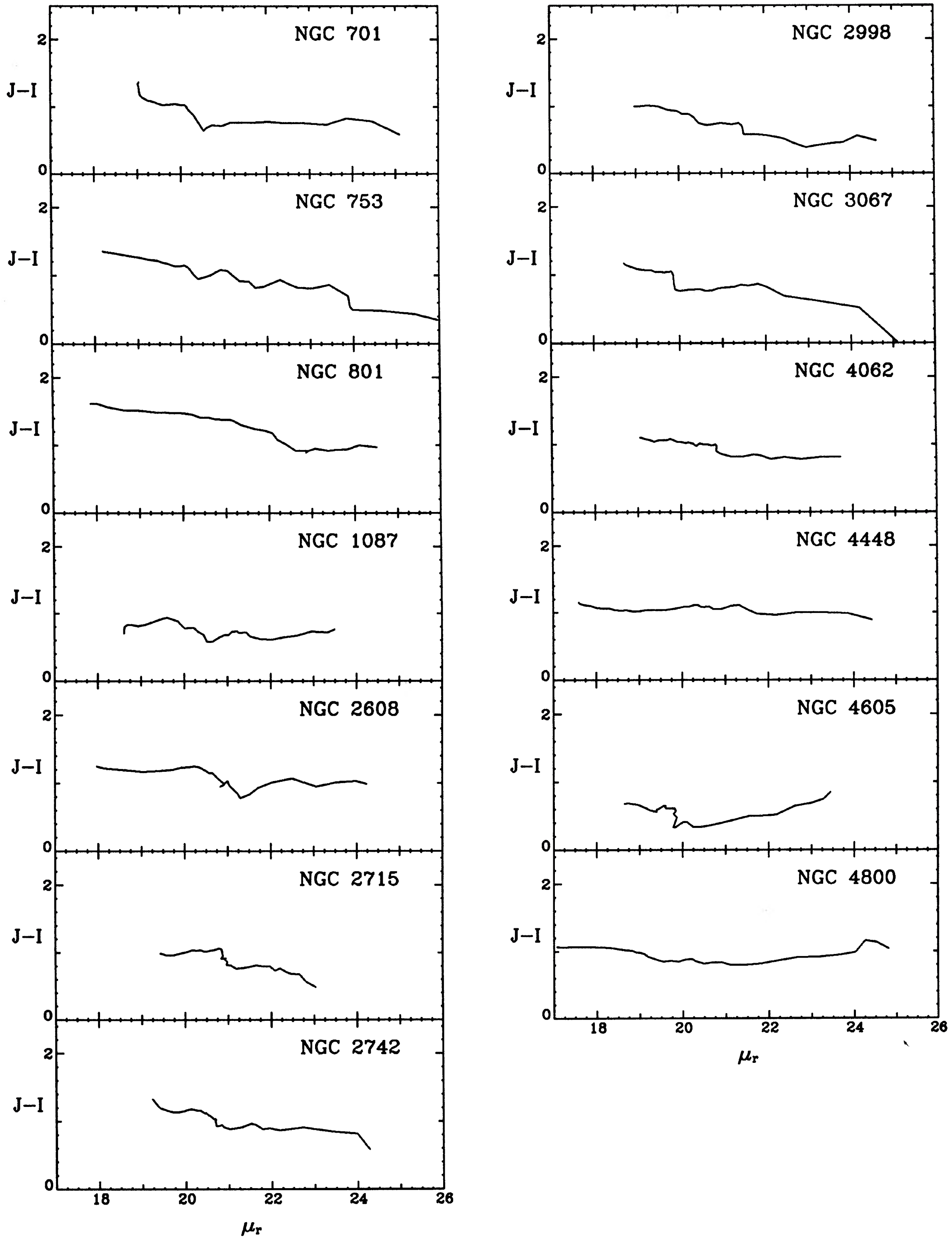

FIG. 1. $J-I$ color gradients for 13 spiral galaxies plotted as a function of surface brightness.

process is repeated until convergence is achieved. Substituting the solution back into Eq. (1), the disk profile can be determined as well.

This decomposition has been applied to all but five galaxies with significant bulge components. Bulge and disk eccentricities $\epsilon_B$ and $\epsilon_D$ are taken from the run of ellipticity with radius in each galaxy: $\epsilon_B$ is set equal to the minimum ellipticity in the center and $\epsilon_D$ to the average ellipticity at large radii. These ellipticities are listed in Table I. In the remaining five galaxies, the decomposition was not satisfactory because the galaxy is too face-on for the method to work, or the bulge and disk have nearly equal apparent flattenings. In these cases, the standard method of using fitting functions has been applied.

Several factors influence the reliability of the decomposition. The bulge flattening is not always well determined because the bulge does not always dominate even in the center. Seeing can distort the inner profile. The influence of these factors on individual components is not easy to assess, but a visual examination of the resulting decompositions suggests no serious problems. Nonaxisymmetric structure in the disk and a change in flattening with radius in the bulge will also cause systematic errors in the derived profiles; problems of the first type are apparent in the bulge component for a few galaxies where the bulge profiles appear bumpy and can even have secondary maxima. Such erratic and unphysical behavior always occurs in regions where the disk dominates and so will have little effect on the rotation-curve calculations which follow.

The one source of error that can be checked numerically is the influence of the choice of bulge- and disk-flattening parameters on the decomposition. Qualitatively, increasing the bulge flattening increases the fraction of light near the galaxy center attributed to the bulge. Similarly, increasing the disk flattening increases the amount of light attributed to the bulge at large radii. The disk flattening is in fact selected to force the bulge to reach zero intensity at a finite radius.

The decompositions are plotted in the upper panels in Fig. 2. In all but a few cases, they "look" reasonable, the disk intensity continues into the center at roughly constant intensity, while the bulge dominates the light in the center and falls off smoothly in the disk-dominated region. The bulge profiles are nowhere close to an $r^{1/4}$ law (a situation almost guaranteed by the decomposition procedure).

The influence of an error in the bulge/disk decompositions on the rotation curves will be discussed later in Sec. VI.

## V. ROTATION-CURVE MODELS

The mass distribution in a spiral galaxy is modeled as the sum of three discrete components: the bulge, disk, and halo. The bulge and disk mass distributions are presumed to be given by their respective luminosity distributions to within an unknown mass/light ratio, which is assumed to be constant within each component. The halo mass distribution can be either parametrized or derived from the observed rotation curve. The bulge and halo are assumed to be spherically symmetric and the disk to be infinitely thin.

The rotation velocity $v_c$ in a galaxy at a radius $r$ is given by

$$v_c^2(r) = r(\partial\phi/\partial r),$$

where the gravitational potential $\phi = \phi_{\rm disk} + \phi_{\rm bulge} + \phi_{\rm halo}$. Expressions for each of these terms will now be given.

### a) Disk

Toomre (1963) gives the most elegant approach to computing the rotation curve of a disk. Starting with Poisson's equation in cylindrical coordinates:

$$\frac{1}{r}\frac{\partial}{\partial r}\left(r\frac{\partial\phi}{\partial r}\right) + \frac{\partial^2\phi}{\partial z^2} = 4\pi G\rho = 4\pi G\mu(r)\delta(z),$$

one applies a Fourier-Bessel transformation to find

$$\frac{\partial\phi}{\partial r} = 2\pi\int_0^\infty a\mu(a)H(a,r)\,da, \qquad (3)$$

where

$$\begin{aligned} H(a,r) &= \int_0^\infty tJ_0(at)J_1(rt)\,dt \\ &= \frac{2}{\pi ar}\left[K(k) - \frac{E(k)}{1-k^2}\right], \quad k = r/a\,(r<a) \\ &= \frac{2E(k)}{\pi r^2(1-k^2)}, \quad k = a/r\,(a<r). \end{aligned}$$

Here, $\mu(a)$ is the surface density profile and $K(k)$ and $E(k)$ are complete elliptic integrals of the first and second kind, respectively.

The Green's function $H(a,r)$ is positive for $a<r$ and negative for $a>r$ with a singularity at $a=r$. One could integrate Eq. (3) by parts in order to tame the singularity; however, with proper care, the original equation can be integrated numerically without trouble (the singularity is only logarithmic), avoiding the need to compute $d\mu/da$. Nevertheless, the rotation curve is sensitive to bumpiness in the surface density profile as described by $d\mu/dr$. This sensitivity can be used to advantage, as will be discussed later.

### b) Bulge

For a spherically symmetric distribution, one has simply $\partial\phi/\partial r = Gm(r)/r^2$, where $m(r)$ is the mass interior to radius $r$. Since the profile decomposition yields the bulge profile as a projected density $\mu$, two integrations are required to derive $m(r)$:

$$\rho(s) = -\frac{1}{\pi}\int_s^\infty \frac{d\mu}{(x^2-s^2)^{1/2}},$$

$$m(r) = \int_0^r 4\pi s^2\rho(s)\,ds.$$

With some manipulation, these integrals can be combined to yield

$$m(r) = \int_0^r 2\pi x\mu(x)\,dx + \int_r^\infty [(4\sin^{-1}(r/x) - 4r(x^2-r^2)^{-1/2}]\,x\mu(x)\,dx.$$

Corrections for the flattening of the bulge have been ignored.

### c) Halo

The form of the halo density profile is not well constrained *a priori* other than that it produces an asymptotically flat rotation curve. One density law that has this property is

$$\rho = \frac{\rho_0}{1+(r/a)^2} = \frac{\sigma^2}{2\pi G(r^2+a^2)}, \qquad (4)$$

where $\rho_0$ (or $\sigma$) and $a$ are adjustable constants. This profile produces a rotation curve

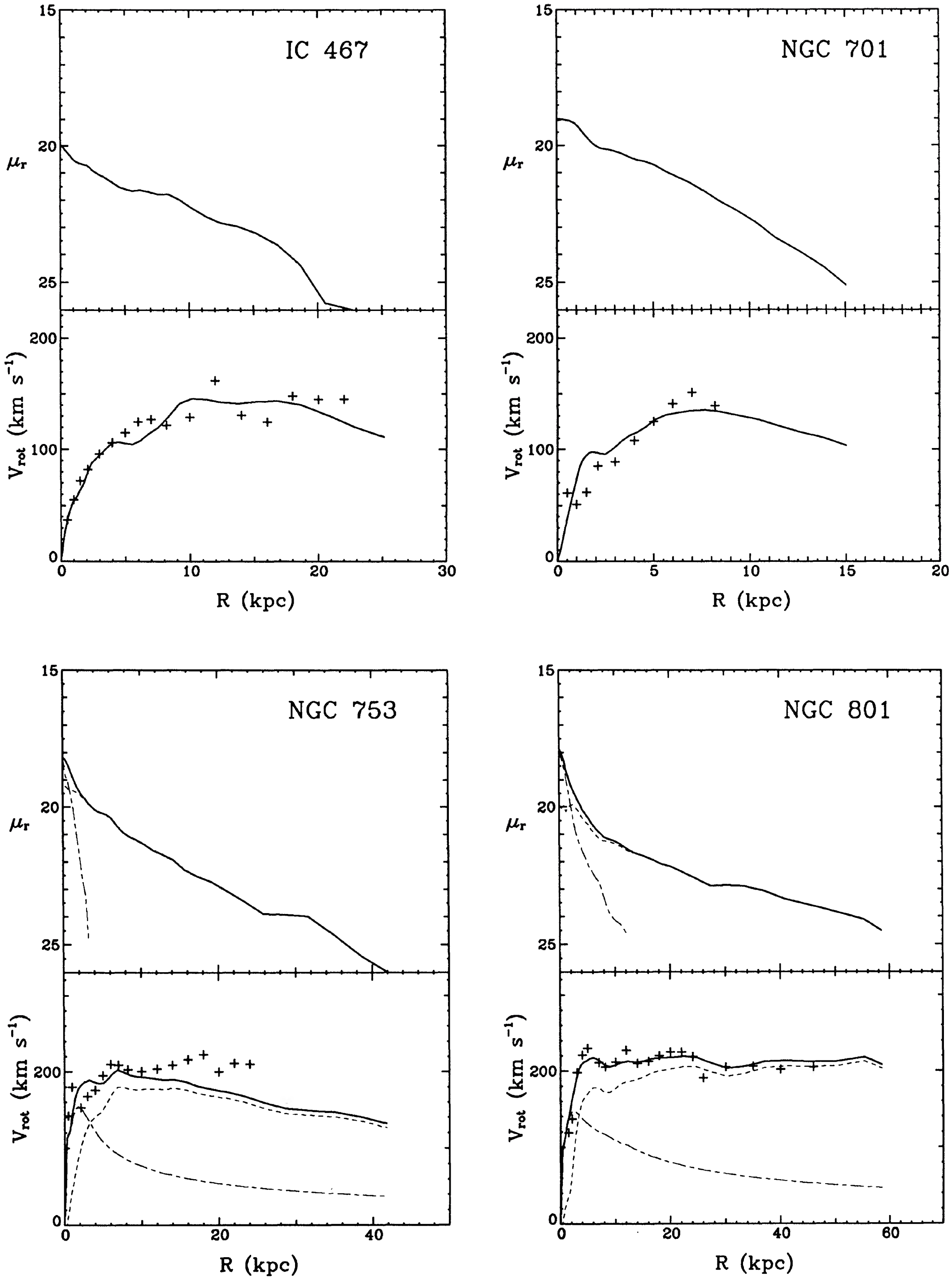

FIG. 2. Top panels: Major-axis luminosity profiles for 37 spiral galaxies. The profile is decomposed into bulge (short- and long-dashed) and disk (short-dashed) components. Lower panels: Observed rotation curves (pluses) and the best-fitting maximum-disk solution (solid line). The separate contributions of the bulge and disk components are also drawn.

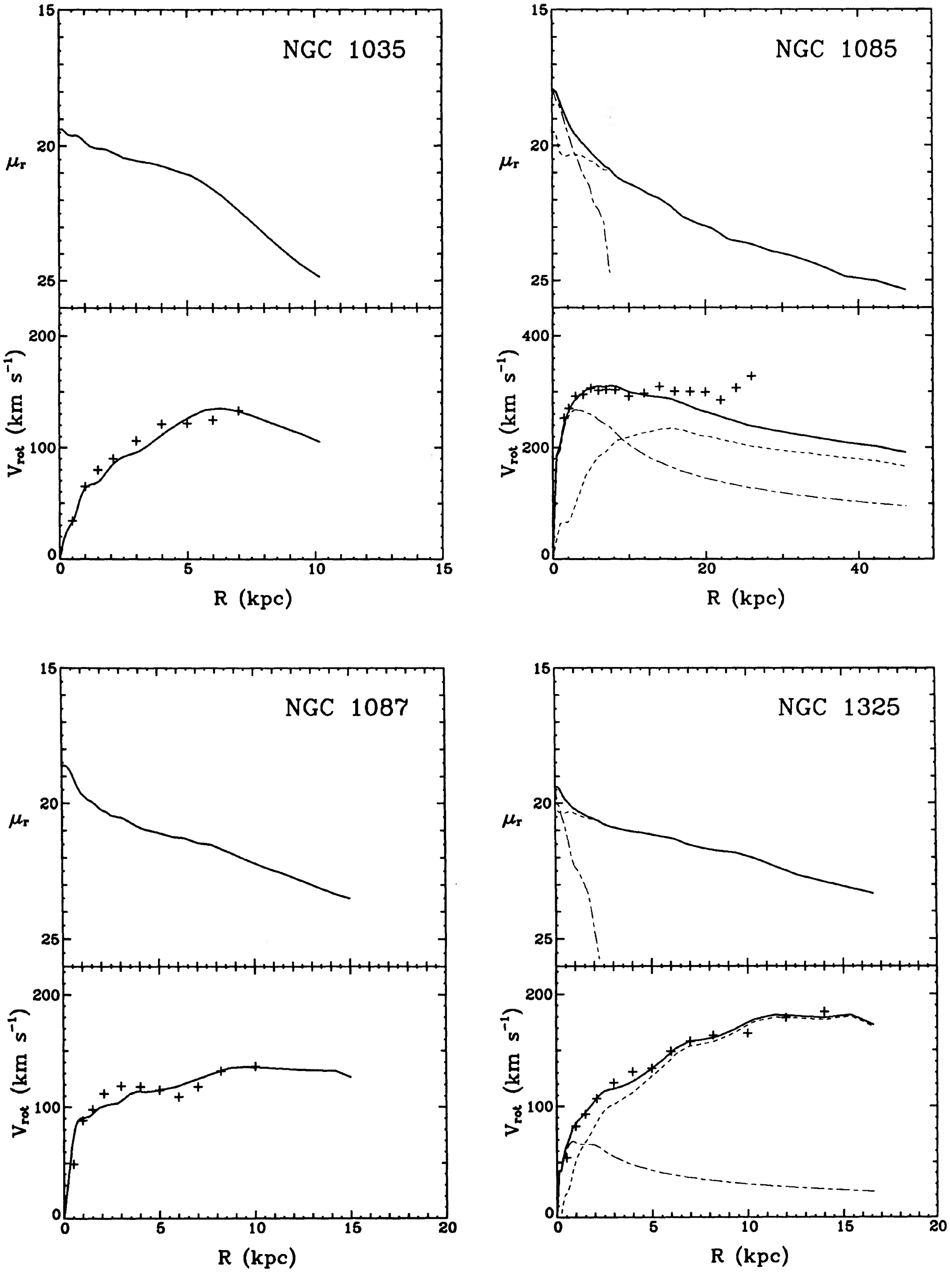

FIG. 2. (continued)

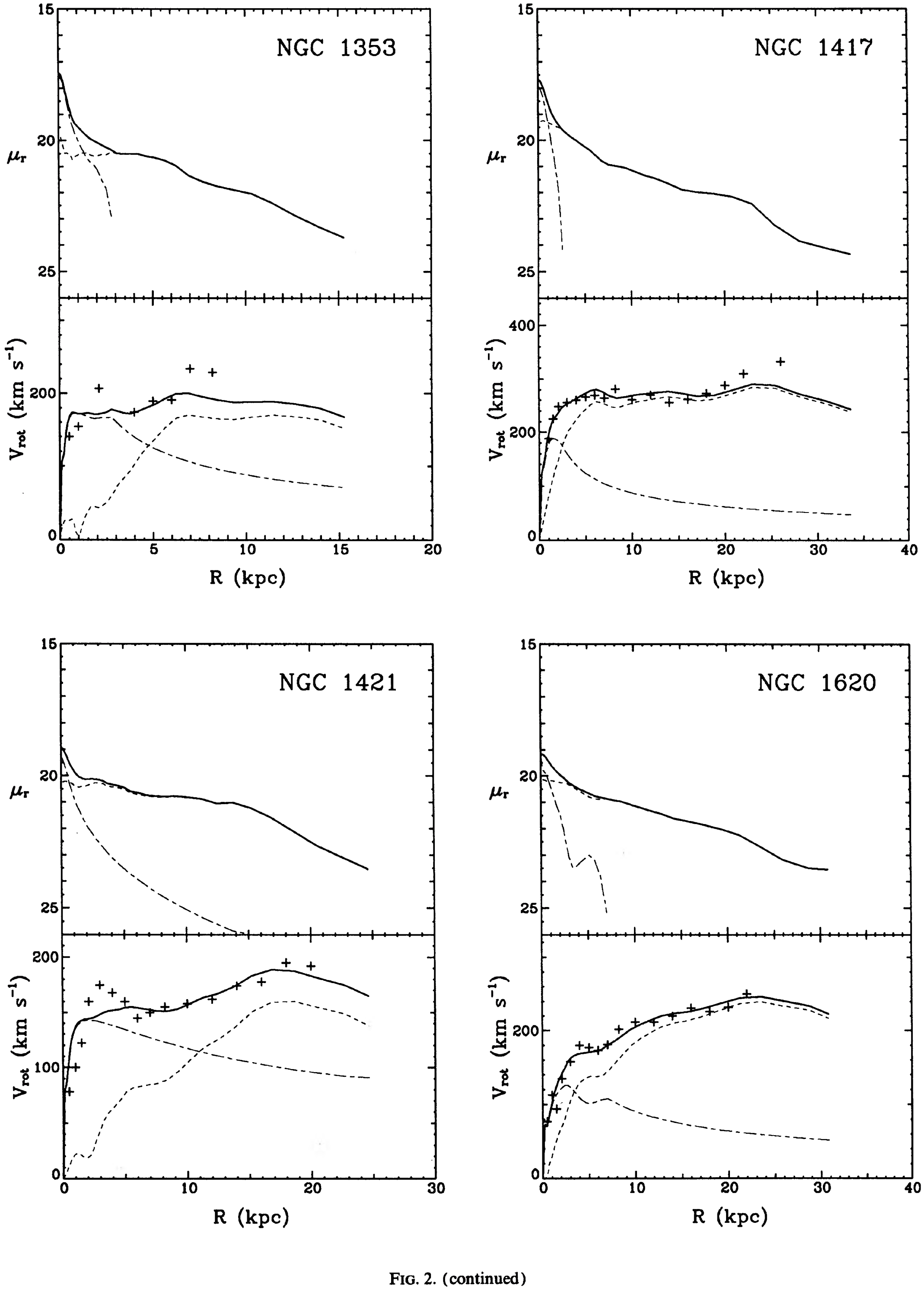

FIG. 2. (continued)

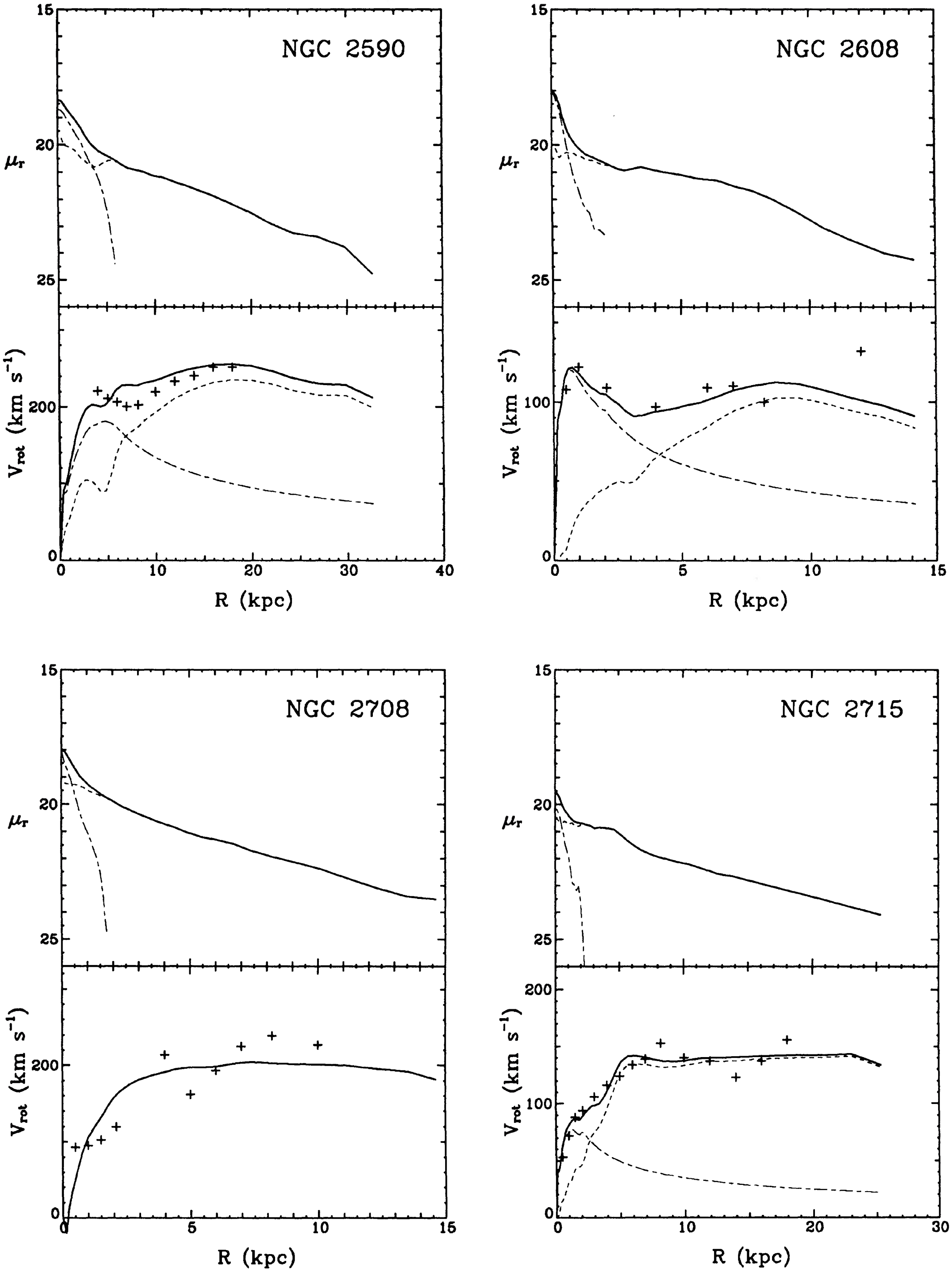

FIG. 2. (continued)

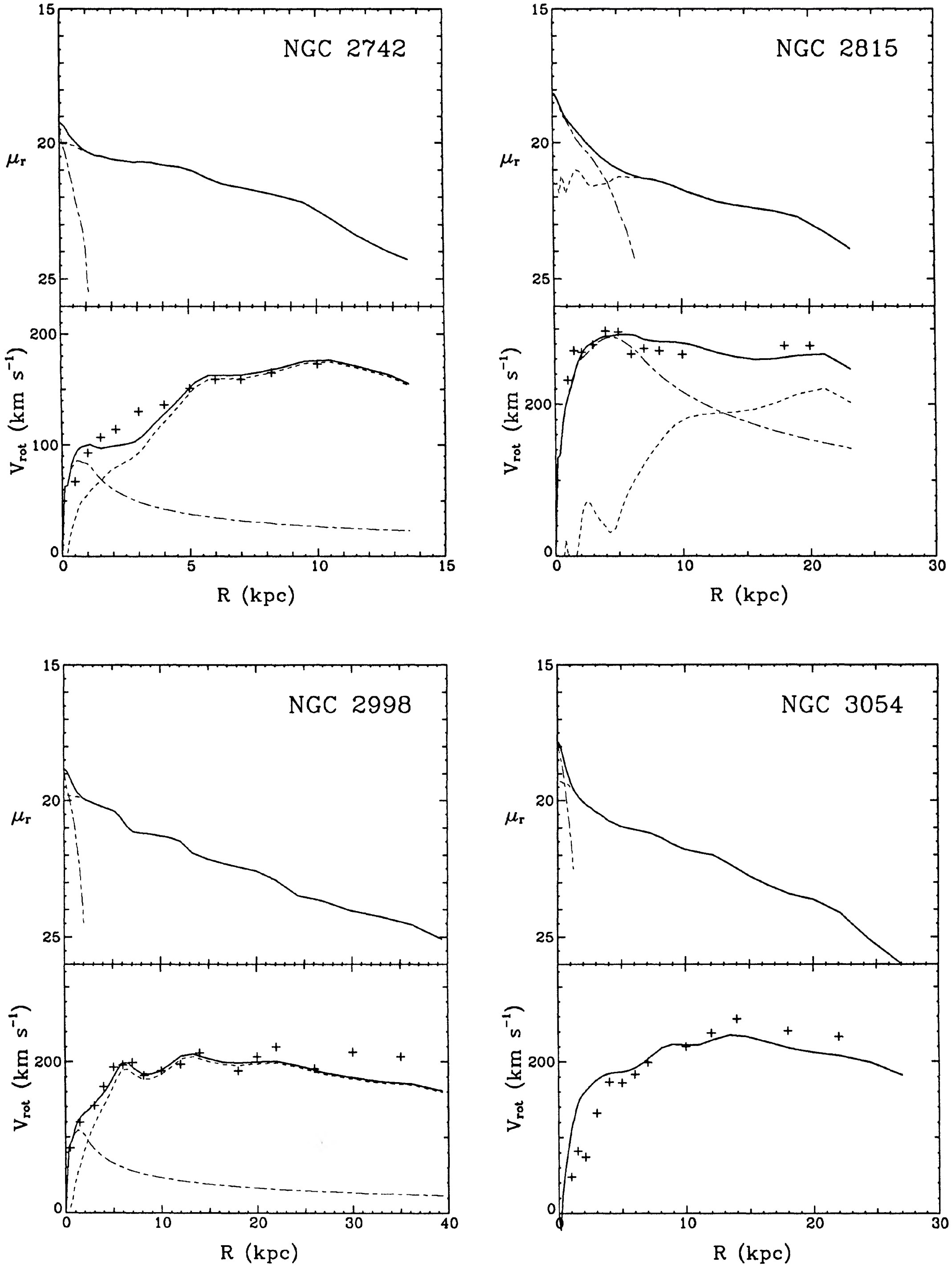

FIG. 2. (continued)

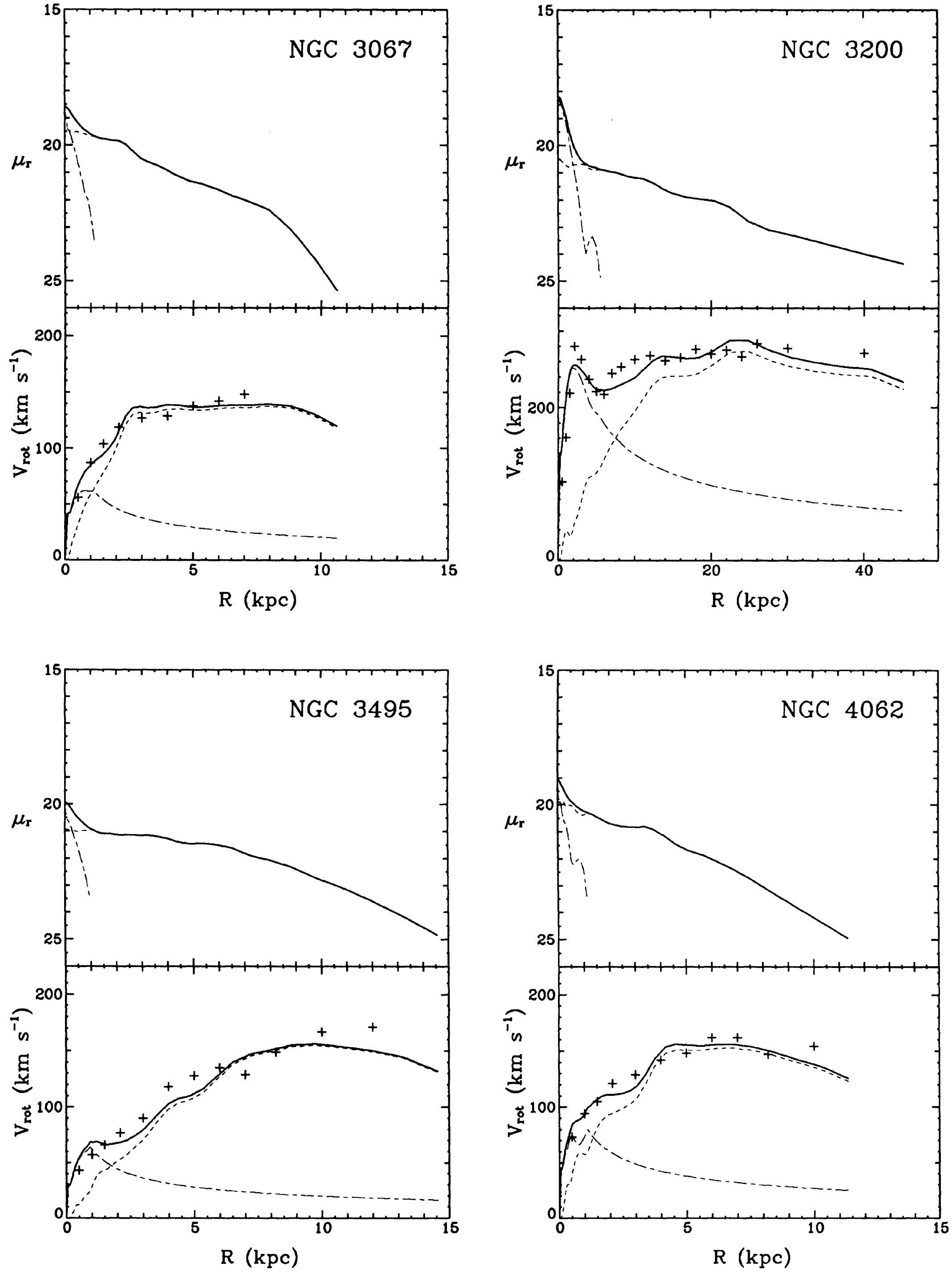

FIG. 2. (continued)

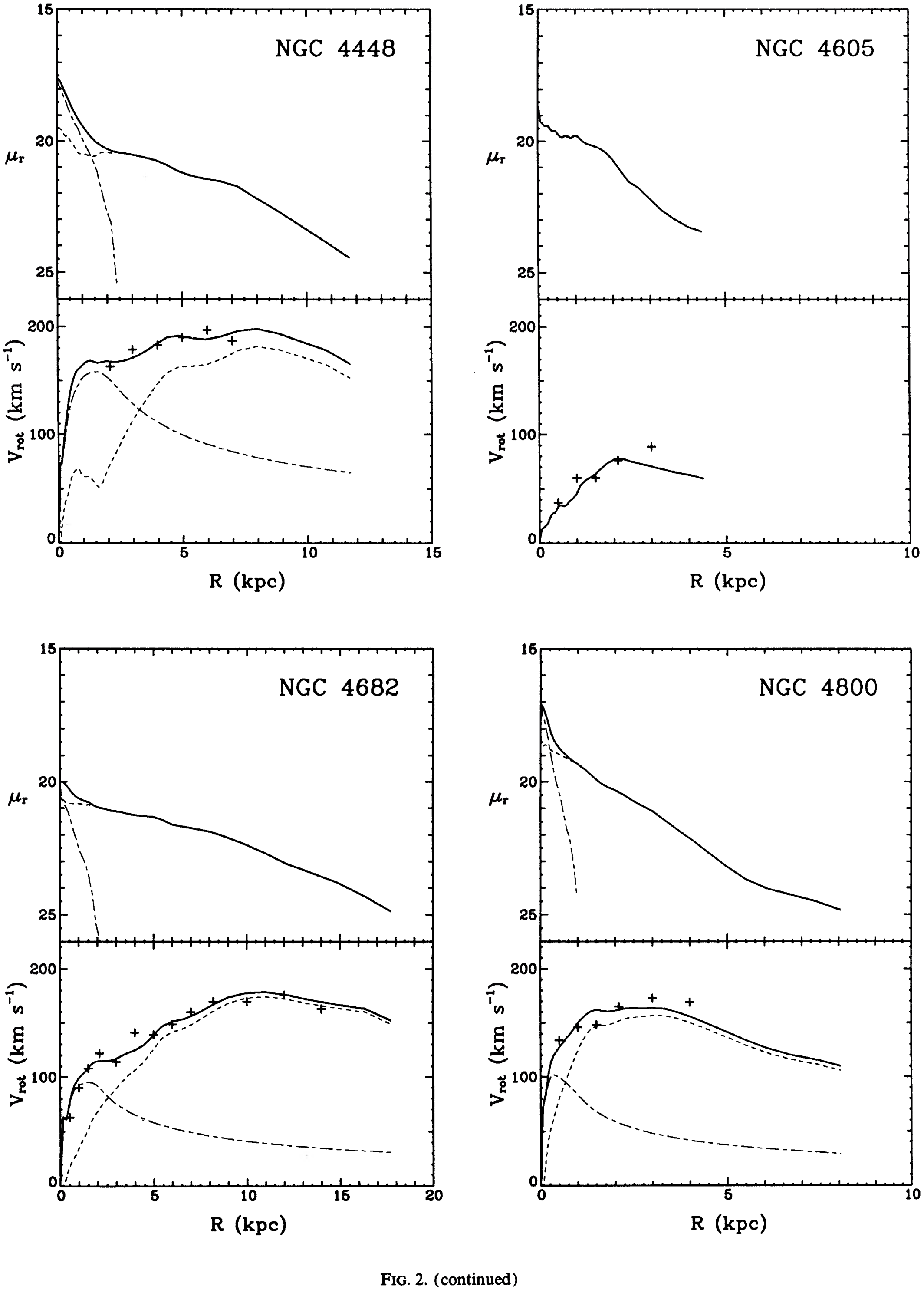

FIG. 2. (continued)

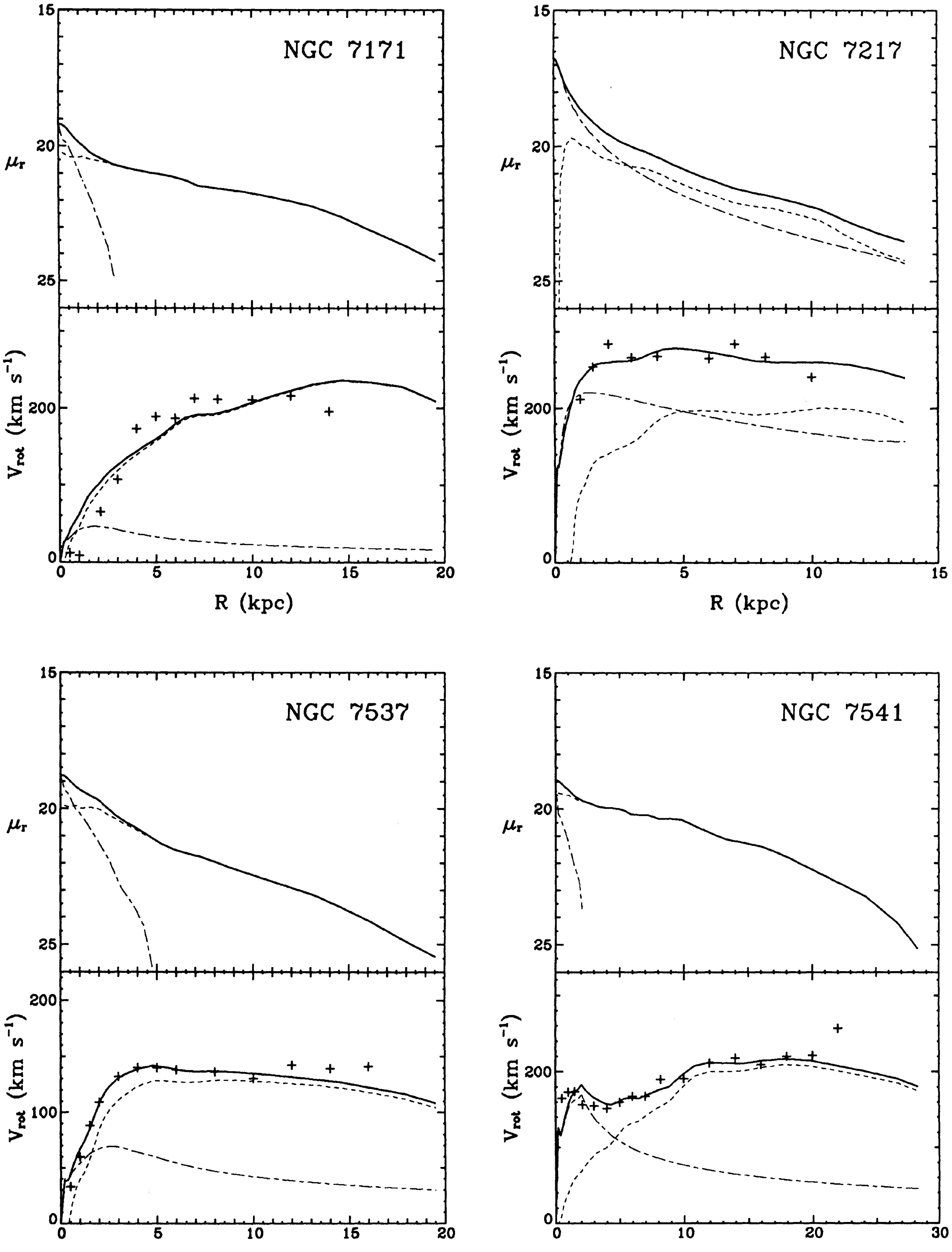

FIG. 2. (continued)

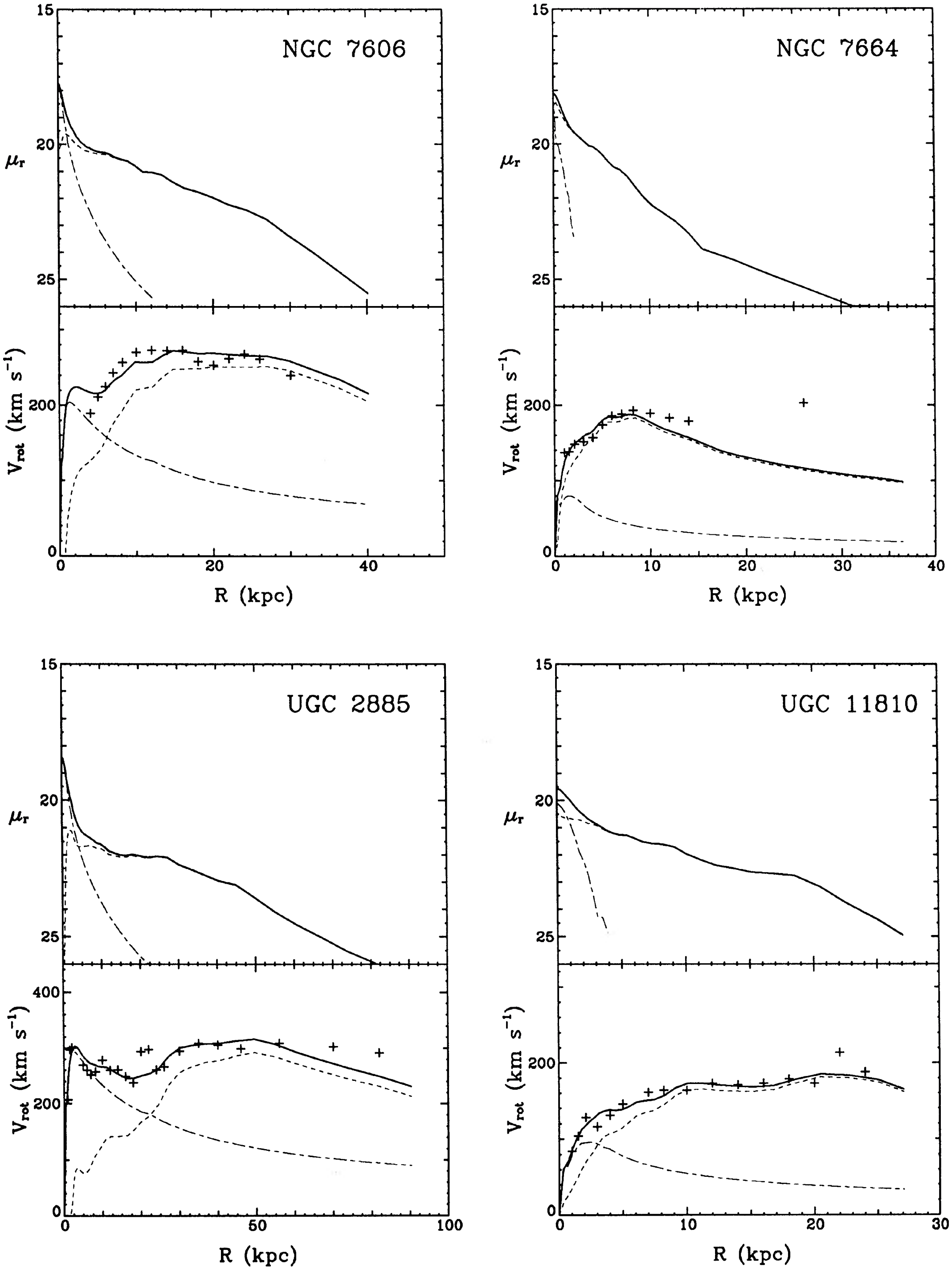

FIG. 2. (continued)

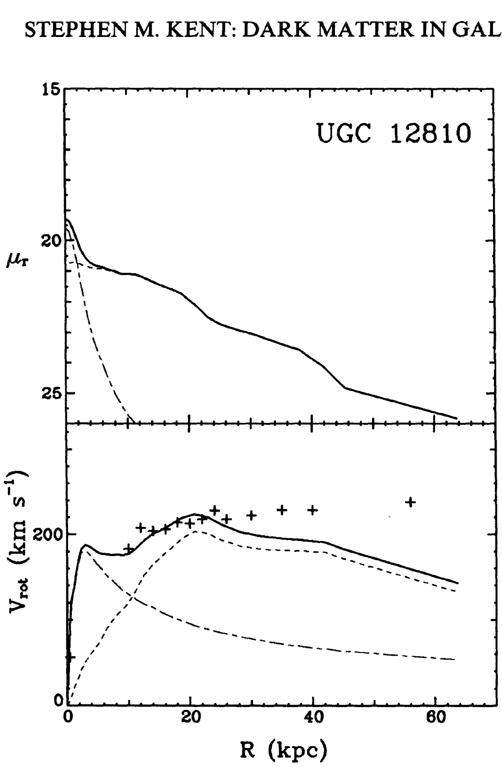

FIG. 2. (continued)

$$v_c^2\ (r) = 2\sigma^2[1 - (a/r)\tan^{-1}(r/a)]\ ,$$

with an asymptotic velocity of $\sqrt{2}\sigma$. Alternative profiles (e.g., an isothermal sphere) could be used, but there is no reason to select one over the other (if the halo *did* have the profile of an isothermal sphere, it would not, in fact, be isothermal itself since it is embedded in the potential well of the disk and bulge).

## VI. MODEL FITTING

### a) Method

In principle, matching the rotation curve models to the observed profiles is straightforward. For any galaxy, a model rotation curve is computed from the observed bulge and disk profiles and the assumed halo profile: $v_c^2(r) = v_B^2 + v_D^2 + v_H^2$. Four free parameters, the bulge and disk M/L ratios and the scale parameters $\sigma$ and $a$ for the halo, are adjusted by a least-squares fit to the observed rotation-curve profile (the fit is actually made to $v_c^2$). The dependence of $v_c$ on $a$ is nonlinear, so an iterative fit needs to be done.

In practice, it is found that if a fit is made solving for all four parameters simultaneously, the solution is nearly singular. The problem is that the observed rotation curves do not extend far enough to decouple the interdependence of the disk M/L ratio and halo parameters. Consequently, it is necessary to constrain the disk or halo parameters in some way. Several methods have been tried.

#### 1) Maximum-disk method

In this method (similar to that used by van Albada *et al.* 1985) it is assumed that the stellar component dominates the mass distribution in the inner part of a galaxy. The M/L ratio for the disk (and bulge) are set to the maximum value consistent with matching the inner part of the rotation curve. Any excess in rotation velocity at large radii is then attributed to a dark halo component. This method is implemented by ignoring the halo component and solving for the bulge and disk M/L ratios in a region inside the radius at which the rotation velocity due to the disk component alone reaches a maximum.

#### 2) Fixed-σ method

This approach is motivated by the fact that 21 cm measurements show that rotation curves usually remain flat well beyond the optical edge of a galaxy. If the asymptotic velocity $v_c$ is known, then the halo parameter $\sigma$ can be set to a value $v_c(\infty)/\sqrt{2}$. For most galaxies, this velocity can be determined reasonably well by inspection. For a few (especially those of low luminosity), an estimate of $v_c$ has been obtained by fitting a pure halo model to the observed velocity curve. With $v_c$ (and $\sigma$) so determined, the remaining three parameters are found by a least-squares fit.

#### 3) Constant-density halo

It was found using method (2) that the optical rotation curves seldom extend past the solid-body rotation part of the halo density profile. Consequently, a set of fits has been made with a constant density for the halo. This method also has the advantage that it requires only one free parameter for the halo.

### b) Results

The parameters determined by these three methods are listed in Tables III–V, respectively. Most of the columns are self-explanatory. Masses and luminosities are in units of $10^{10}$ $M_\odot$ and $10^{10}$ $L_\odot$, respectively. The individual mass/light ratios for the bulge and disk are not corrected for internal or foreground extinction. In Table III, column (4) gives the radius at which the velocity profile of the disk component peaks, column (5) gives the radius of the last point in the luminosity profile, column (7) gives the total stellar mass inside that point, column (8) gives the apparent luminosity, and column (9) gives the luminosity corrected for foreground extinction. These extinction corrections are taken to be 0.6 times the values given by Burstein *et al.* (1982) and Rubin *et al.* (1982). Although the optical radius in column (5) does not correspond to any standard isophote, it usually lies very close to the blue isophotal radius $R_{25}$ of the RC2 (de Vaucouleurs, de Vaucouleurs, and Corwin 1976). In Table IV, columns (7–9) list the masses of each component inside the radius of the last measured velocity point. For the disk component, column (8), this is actually the quantity $v_D^2\ r/G$; the true mass is usually lower by about 20%. Column (10) gives the (true) total mass inside the optical radius. In Table V, the halo density $\rho_0$ is in units of $10^{-26}$ g cm$^{-3}$. Again, it should be pointed out that the luminosities are *not* corrected for internal extinction (this point will be examined later).

The fits from the maximum-disk solutions are plotted in the lower panels of Fig. 2. For NGC 753 and NGC 2998, the fits from the fixed-$\sigma$ solutions are plotted in Fig. 3.

Several points can be made:

(1) The three methods can give widely differing solutions for the various parameters.

(2) The maximum-disk solutions (with no halo) provide good fits over the entire velocity profile for many objects. In other objects, the maximum-disk solutions fall short only for the last few observed velocity points.

1986AJ.....91.1301K

TABLE III. Maximum-disk solutions.

| Name<br>(1) | $(M/L)_B$<br>(2) | $(M/L)_D$<br>(3) | $R_{max}$ kpc<br>(4) | $R_{opt}$ kpc<br>(5) | rms km/s<br>(6) | $M_*$(opt)<br>(7) | $L_*$(opt)<br>(8) | $L_*$(cor)<br>(9) |
|---|---|---|---|---|---|---|---|---|
| I467 | - | 3.48 | 10.3 | 25.3 | 9 | 6.1 | 1.8 | 1.9 |
| N701 | - | 1.50 | 7.7 | 15.3 | 18 | 3.1 | 2.1 | 2.1 |
| N753 | 2.76 | 1.21 | 6.9 | 42.1 | 23 | 14.4 | 11.3 | 12.6 |
| N801 | 1.47 | 6.91 | 55.3 | 58.6 | 11 | 42.6 | 7.8 | 8.7 |
| N1035 | - | 2.80 | 6.3 | 10.2 | 7 | 2.1 | 0.75 | 0.86 |
| N1085 | 3.59 | 2.70 | 15.5 | 46.5 | 8 | 34.7 | 11.9 | 12.7 |
| N1087 | - | 1.26 | 9.6 | 15.2 | 10 | 4.1 | 3.2 | 3.4 |
| N1325 | 4.26 | 4.91 | 15.4 | 16.6 | 5 | 8.2 | 1.7 | 1.7 |
| N1353 | 4.23 | 2.91 | 6.9 | 15.3 | 20 | 8.0 | 2.6 | 2.6 |
| N1417 | 2.37 | 3.49 | 23.0 | 33.6 | 11 | 36.6 | 10.7 | 11.5 |
| N1421 | 9.22 | 2.17 | 18.6 | 24.7 | 17 | 12.7 | 4.2 | 4.6 |
| N1620 | 4.14 | 4.39 | 23.5 | 30.9 | 10 | 26.4 | 6.0 | 6.7 |
| N2590 | 3.50 | 4.54 | 20.0 | 32.6 | 13 | 25.8 | 6.1 | 6.5 |
| N2608 | 3.04 | 0.79 | 8.6 | 14.1 | 7 | 2.2 | 2.4 | 2.5 |
| N2708 | -0.63 | 4.61 | 7.4 | 14.6 | 37 | 8.6 | 2.0 | 2.0 |
| N2715 | 4.53 | 2.38 | 23.0 | 25.4 | 9 | 8.2 | 2.0 | 3.4 |
| N2742 | 8.42 | 2.72 | 10.5 | 13.6 | 12 | 5.5 | 2.0 | 2.2 |
| N2815 | 6.83 | 6.63 | 21.1 | 23.2 | 17 | 26.1 | 3.9 | 5.4 |
| N2998 | 3.59 | 2.53 | 13.3 | 39.4 | 7 | 19.3 | 7.6 | 7.6 |
| N3054 | -2.72 | 3.73 | 13.4 | 27.0 | 21 | 16.5 | 4.7 | 5.4 |
| N3067 | 2.89 | 2.27 | 8.0 | 10.6 | 7 | 2.8 | 1.2 | 1.2 |
| N3200 | 5.30 | 7.78 | 24.8 | 45.3 | 22 | 47.0 | 6.3 | 7.3 |
| N3495 | 7.33 | 7.69 | 10.0 | 14.9 | 11 | 4.8 | 0.62 | 0.96 |
| N4062 | 5.85 | 4.22 | 7.0 | 11.6 | 8 | 3.6 | 0.83 | 0.83 |
| N4448 | 2.93 | 4.53 | 8.0 | 11.7 | 6 | 6.0 | 1.5 | 1.8 |
| N4605 | - | 1.13 | 2.2 | 4.4 | 8 | 0.30 | 0.26 | 0.26 |
| N4682 | 12.6 | 3.87 | 11.0 | 17.7 | 8 | 7.3 | 1.8 | 1.9 |
| N4800 | 1.82 | 1.97 | 3.0 | 8.0 | 8 | 2.0 | 1.0 | 1.0 |
| N7171 | 0.97 | 5.10 | 14.6 | 19.6 | 28 | 14.7 | 3.0 | 3.4 |
| N7217 | 2.72 | 2.76 | 10.4 | 13.7 | 15 | 15.7 | 5.7 | 7.2 |
| N7537 | 1.22 | 3.15 | 8.8 | 19.5 | 5 | 4.4 | 1.6 | 1.7 |
| N7541 | 19.5 | 2.17 | 17.9 | 28.3 | 15 | 16.6 | 7.1 | 7.9 |
| N7606 | 5.96 | 3.20 | 27.0 | 40.1 | 12 | 36.1 | 10.6 | 11.7 |
| N7664 | 2.40 | 1.57 | 8.4 | 36.5 | 7 | 7.5 | 4.7 | 5.1 |
| U2885 | 7.18 | 5.52 | 49.6 | 90.4 | 19 | 98.1 | 17.1 | 51.6 |
| U11810 | 4.27 | 4.07 | 20.5 | 27.1 | 8 | 12.8 | 3.1 | 3.2 |
| U12810 | 6.14 | 2.58 | 20.8 | 63.7 | 22 | 29.3 | 10.4 | 11.1 |

(3) The fixed-$\sigma$ solutions show a large scatter in the nature of the fits, ranging from halo dominated in some objects to no halo at all in others. However, the solutions are usually highly degenerate, and widely varying sets of parameters can give nearly equally good fits for most objects. Consequently, little weight should be given to the individual parameters in Table IV. Nevertheless, the composite rotation curves provide a convenient "French curve" fit to the observed rotation curves and are useful in extrapolating the mass profiles to larger radii. The fits to NGC 753 and NGC 2998 shown in Fig. 3 are examples of two of the better-determined solutions.

(4) The constant-density halo solutions are usually intermediate in the ratio of halo mass to stellar mass between the constant-$\sigma$ and maximum-disk solutions.

(5) Few measured rotation curves extend much beyond the peak in the predicted disk portion of the rotation curve (only five extend to as far as twice the radius of the peak). Hence the curves are never in the region of a true Keplerian dropoff in velocity.

(6) Disk profiles are not always well represented by an exponential law, and consequently the resulting rotation curves do not behave the way one would expect based upon the exponential law. An excellent example is NGC 801, where the disk rotation curve is remarkably flat over most of its range.

(7) Ten objects are best fit with no halo by all three methods. They include NGC 7217, a galaxy already analyzed by Kalnajs (1983) with the same result. The largest is NGC 801, whose rotation curve extends past 40 kpc.

(8) Several objects stand out as anomalous. NGC 7171 could not be fit well by any combination of bulge/disk/halo. NGC 3054 could only be fit with negative bulge M/L ratio. The fit for this galaxy drawn in Fig. 2 excludes the bulge contribution. For UGC 12810, the maximum-disk solution gives a very poor fit; however, this object is well fit with a dominant halo and an essentially massless disk. NGC 701 and NGC 2708 are likewise best fit with a dominant halo as produced by the fixed-$\sigma$ solution, but in these cases the bulge and disk M/L ratios are significantly different from 0. However, the anomalous behavior shown by these galaxies may not always be significant: many galaxies (including NGC 2708, NGC 3054, and NGC 7171) have asymmetric velocity profiles, indicating that the rotation curves for these objects may deviate significantly from the true circular velocity profile.

(9) With one exception (UGC 12810), nowhere does the rotation curve for any object reach the asymptotic flat part of the halo. Rather the flat nature of the measured curves is due more to the form of the bulge + disk profiles. (It should be emphasized that few rotation curves are truly flat, especially when the physically more relevant quantity $v_c^2$ is plotted against radius.)

The inner few points of the measured rotation curve sometimes do not match the predicted profile very well. Seeing usually influences the first point of both the observed velocity profile and that derived from the photometric profile. It is also possible that the inner points are influenced by noncircular motions. At least two galaxies, NGC 701 and NGC 1087, have bars in their centers, where circular motion is not even possible. A good example of a nearby galaxy with noncircular motions in the inner rotation curve is M81 (Goad 1976).

Overall, the optical rotation curves do not pin down the individual halo parameters or stellar M/L ratios very well. However, as will be discussed in Sec. VII, the maximum-disk solutions most likely provide the best estimate of the stellar M/L ratio.

One last point that needs to be discussed is the effect of decomposition errors and color gradients on the solutions. The effect of decomposition errors was checked by repeating the decomposition of the luminosity profiles for a few galaxies using different values for the bulge and disk ellipticity. Although the individual bulge and disk profiles were changed, the resulting M/L ratios and halo parameters varied typically by no more than 10%. The effect of color gradients was checked by again repeating the entire decomposition and least-squares fitting procedures for NGC 753 but using first the *J* and then the *I* luminosity profiles. The results were as expected: Since the *J* profile declines less steeply than the *I* profile, the predicted stellar rotation curve from the *J* profile peaks at a larger radius, and the solutions for stellar and halo masses give a relatively larger mass fraction in stars. For example, the halo mass derived by the fixed-$\sigma$ solution increases by 50% between the *J* and *I* profiles. Consequently, for this galaxy, the assumption of constant M/L ratio in the disk is probably not very good. Ideally one would like to make observations in a bandpass that most closely reflects the underlying stellar mass distribution. Most likely an infrared bandpass is optimum.

TABLE IV. Fixed-$\sigma$ solutions.

| Name<br>(1) | $(M/L)_B$<br>(2) | $(M/L)_D$<br>(3) | $\sigma$<br>(4) | a kpc<br>(5) | rms km/s<br>(6) | $M_B$<br>(7) | $M_D$<br>(8) | $M_H$<br>(9) | $M_T$(opt)<br>(10) |
|---|---|---|---|---|---|---|---|---|---|
| I467 | – | 3.36 | 108 | 31.9 | 11 | – | 7.7 | 1.5 | 8.0 |
| N701 | – | 0.59 | 133 | 4.3 | 12 | – | 1.4 | 2.9 | 9.2 |
| N753 | 2.87 | 1.04 | 148 | 10.9 | 15 | 1.4 | 11.2 | 11.6 | 40.6 |
| N801 | 1.47 | 6.91 | – | – | 11 | 3.0 | 44.9 | – | 42.6 |
| N1035 | – | 2.80 | – | – | 7 | – | 2.9 | – | 2.1 |
| N1085 | 3.80 | 0.81 | 219 | 7.0 | 9 | 10.3 | 7.4 | 37.2 | 98.4 |
| N1087 | – | 1.26 | – | – | 10 | – | 4.3 | – | 4.1 |
| N1325 | 4.26 | 4.91 | 138 | – | 5 | .2 | 10.2 | – | 8.2 |
| N1353 | 3.68 | 1.71 | 153 | 3.5 | 18 | 1.6 | 3.1 | 4.5 | 16.7 |
| N1417 | 2.66 | 3.01 | 205 | 19.8 | 12 | 2.0 | 40.2 | 15.1 | 57.4 |
| N1421 | 9.04 | 0.52 | 141 | 8.0 | 16 | 4.2 | 2.7 | 9.6 | 20.0 |
| N1620 | 4.14 | 4.39 | – | – | 10 | 1.9 | 28.7 | – | 26.4 |
| N2590 | 3.67 | 2.42 | 180 | 10.9 | 11 | 6.3 | 10.2 | 10.2 | 45.3 |
| N2608 | 2.97 | 0.14 | 90 | 3.0 | 8 | 0.4 | 0.4 | 3.0 | 4.5 |
| N2708 | 0.84 | 0.82 | 191 | 2.8 | 19 | 0.1 | 1.7 | 10.8 | 19.9 |
| N2715 | 4.58 | 2.30 | 107 | 36.7 | 9 | 0.3 | 7.8 | 0.7 | 9.5 |
| N2742 | 8.42 | 2.72 | – | – | 12 | 0.2 | 7.0 | – | 5.5 |
| N2815 | 6.85 | 3.38 | 196 | 13.5 | 14 | 10.9 | 11.1 | 12.0 | 35.0 |
| N2998 | 3.79 | 2.39 | 151 | 29.0 | 9 | 0.5 | 22.1 | 10.0 | 31.2 |
| N3054 | −2.27 | 3.32 | 196 | 17.6 | 16 | −0.4 | 19.6 | 11.0 | 31.6 |
| N3067 | 3.63 | 1.79 | 111 | 6.4 | 7 | 0.1 | 2.4 | 1.0 | 4.5 |
| N3200 | 4.40 | 1.10 | 193 | 3.5 | 16 | 3.7 | 7.6 | 59.9 | 78.7 |
| N3495 | 4.12 | 0.22 | 146 | 3.3 | 5 | 0.1 | 0.2 | 7.5 | 10.4 |
| N4062 | 6.37 | 3.85 | 119 | 13.1 | 7 | 0.2 | 4.1 | 1.0 | 4.6 |
| N4448 | 2.93 | 4.53 | – | – | 6 | 1.1 | 5.0 | – | 6.0 |
| N4605 | – | – | 80 | 1.0 | 5 | – | – | 0.5 | 0.92 |
| N4682 | 12.8 | 3.81 | – | – | 7 | 0.4 | 8.8 | – | 7.2 |
| N4800 | 2.51 | 0.58 | 124 | 1.0 | 4 | 0.2 | 0.6 | 1.9 | 5.5 |
| N7171 | No fit | | | | | | | | |
| N7217 | 2.72 | 2.76 | – | – | 15 | 6.5 | 9.2 | – | 15.7 |
| N7537 | 1.39 | 2.83 | 106 | 15.1 | 6 | 0.5 | 4.6 | 1.9 | 7.0 |
| N7541 | 20.4 | 0.76 | 175 | 6.9 | 15 | 1.4 | 7.2 | 18.7 | 33.8 |
| N7606 | 6.15 | 3.13 | – | – | 13 | 4.5 | 40.9 | – | 35.6 |
| N7664 | 4.28 | 0.97 | 139 | 5.8 | 6 | 0.6 | 4.8 | 16.2 | 30.3 |
| U2885 | 6.85 | 1.98 | 200 | 13.2 | 15 | 16.1 | 35.5 | 117. | 177. |
| U11810 | 4.27 | 4.07 | 137 | 30.1 | 9 | 0.7 | 16.4 | 3.2 | 16.5 |
| U12810 | 1.39 | 0.09 | 172 | 3.9 | 4 | 1.0 | 1.0 | 68.6 | 80.8 |

## VII. DISCUSSION

### *a) Correlations with Mass/Light Ratio*

A casual inspection of Tables III–V shows that there is a large scatter in the values of the derived parameters. By looking at various correlations, however, some of this scatter can be reduced.

Significant correlation exists between $(M/L)_*$, $M_*$, $\epsilon_D$, and morphological type $T$. $(M/L)_*$ is taken from the maximum-disk solutions in Table III, columns (7) and (9), and is equal to $(M_B + M_D)/(L_B + L_D)$. Of the three solutions listed in Tables III–V, the maximum-disk solution gives the smallest scatter in these relations. A formal least-squares fit gives

$$\begin{array}{llllll} \log (M/L)_* & = 0.15 \log M_* & - 0.63 \log (1-\epsilon_D) & - 0.64 \log T & + 0.43 \\ & \pm 0.05 & \pm 0.14 & \pm 0.23 & \pm 0.16\,, \end{array}$$

where $T = 3$ for Sb's and 5 for Sc's. The rms scatter in $\log (M/L)_*$ is 0.13. UGC 2885 was deleted in this fit because of its large correction for foreground extinction.

The correlation between M/L ratio and mass (or luminosity) has been implicitly known for years, especially with regard to the Tully-Fisher relation (see, for example, Tully, Mould, and Aaronson 1982). [Rubin *et al.* (1982) find no correlation between the total M/L ratio inside an isophotal radius and the blue luminosity, but the scatter in their relation between total mass and blue luminosity is larger than that found here.] The correlation with disk inclination is presumably due to the effect of internal extinction. In Fig. 4, the relation between $(M/L)_*$ (with the luminosity and morphological-type dependence removed) and $\epsilon_D$ is plotted. If no extinction corrections were needed, the coefficient for this term would be 0. At the opposite extreme, if galaxies are optically thick (Burstein 1985), then this term would have a coefficient of 1. A value as large as 0.63 indicates that large corrections are needed; however, the formal error is still large. For comparison, the RC2 uses a much smaller correction of 0.2 for this coefficient (after converting from the blue to the red bandpass). In principle, the use of $(M/L)_*$ as a

1986AJ.....91.1301K

TABLE V. Constant-density halo solutions.

| Name<br>(1) | $(M/L)_B$<br>(2) | $(M/L)_D$<br>(3) | $\rho_0$<br>(4) | rms km/s<br>(5) |
|---|---|---|---|---|
| I467 | - | 3.33 | 2.7 | 11 |
| N701 | - | 1.09 | 52. | 13 |
| N753 | 2.63 | 1.26 | 11.5 | 16 |
| N801 | 1.47 | 6.91 | - | 11 |
| N1035 | - | 2.80 | - | 7 |
| N1085 | 3.78 | 2.03 | 29.5 | 7 |
| N1087 | - | 1.26 | - | 10 |
| N1325 | 4.32 | 4.87 | 0.9 | 5 |
| N1353 | 4.08 | 1.19 | 193. | 18 |
| N1417 | 2.74 | 2.96 | 18.9 | 12 |
| N1421 | 9.37 | 1.74 | 6.9 | 17 |
| N1620 | 4.14 | 4.39 | - | 10 |
| N2590 | 4.04 | 1.74 | 38.7 | 9 |
| N2608 | 3.10 | 0.49 | 25.7 | 8 |
| N2708 | -0.08 | 3.69 | 93.4 | 25 |
| N2715 | 4.70 | 2.28 | 2.0 | 9 |
| N2742 | 8.42 | 2.72 | - | 12 |
| N2815 | 7.08 | 1.27 | 44.3 | 34 |
| N2998 | 3.77 | 2.42 | 4.4 | 9 |
| N3054 | -2.61 | 3.61 | 13.6 | 18 |
| N3067 | 3.62 | 1.86 | 44.0 | 7 |
| N3200 | 5.30 | 7.67 | 1.7 | 21 |
| N3495 | 7.50 | 6.71 | 21.6 | 11 |
| N4062 | 6.34 | 3.89 | 15.3 | 7 |
| N4448 | 2.93 | 4.53 | - | 6 |
| N4605 | - | 0.81 | 170. | 8 |
| N4682 | 12.8 | 3.81 | - | 7 |
| N4800 | 2.18 | 1.63 | 212. | 5 |
| N7171 | No fit | | | |
| N7217 | 2.72 | 2.76 | - | 15 |
| N7537 | 1.39 | 2.87 | 8.2 | 5 |
| N7541 | 20.6 | 1.66 | 18.6 | 15 |
| N7606 | 6.15 | 3.13 | - | 13 |
| N7664 | 2.61 | 1.49 | 16.1 | 5 |
| U2885 | 7.23 | 5.08 | 1.6 | 18 |
| U11810 | 4.36 | 3.88 | 4.0 | 9 |
| U12810 | 6.03 | 2.39 | 4.2 | 17 |

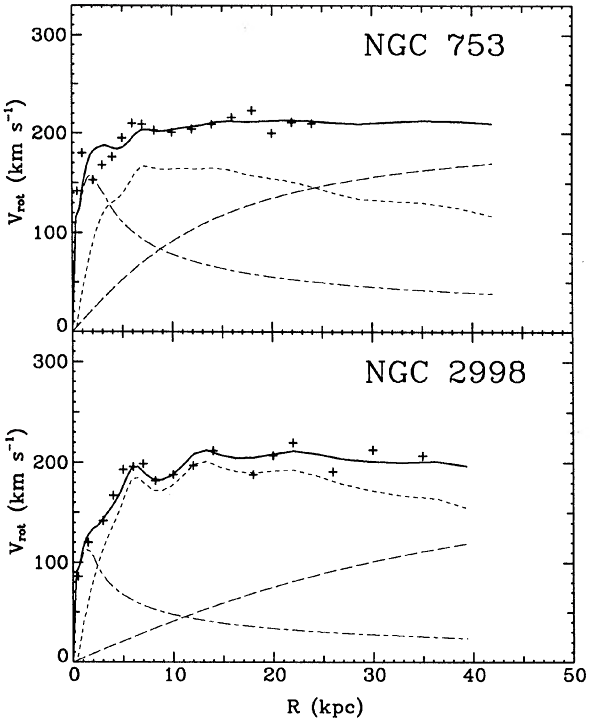

FIG. 3. Best-fitting fixed-$\sigma$ solutions (solid lines) to the observed rotation curves (pluses) of NGC 753 and NGC 2998. The separate contributions of the bulge (short and long dashes), disk (short dashes), and halo (long dashes) are also drawn.

function of inclination is a better method for determining absorption corrections than using surface brightness inside an isophotal radius since the latter method requires measuring the surface brightness inside a radius that itself is a function of inclination. Further, the use of $(M/L)_*$ from the maximum-disk method should be superior to the use of $(M_{\rm Tot}/L)$ since the former does not require measuring $M$ or $L$ alone inside some standard radius. It suffers only from the intrinsic variation in M/L ratio among galaxies and the extra scatter introduced by the not well-known contamination from the halo.

The dependence of M/L ratio on morphological type has also been known previously (cf. Faber and Gallagher 1979). Rubin *et al.* (1982) find that the total M/L ratio for Sb's is a factor 1.7 times that for Sc's in the blue band, compared with a factor 1.4 found here for the stellar component only. The geometric mean of the inclination-corrected M/L ratios at a fiducial mass of $10^{11} M_\odot$ are 1.35 for Sc galaxies and 1.87 for Sb galaxies. Without inclination corrections, these numbers would be a factor 1.75 higher.

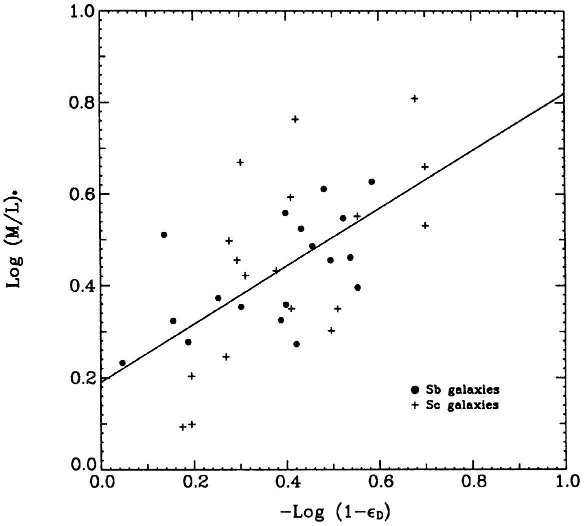

FIG. 4. Correlation between apparent stellar M/L ratio and inclination. The M/L ratios have been corrected for the correlation with mass and morphological type to a galaxy of $10^{11} M_\odot$ and type $T = 4$.

1986AJ.....91.1301K

### *b) Constraints on the Stellar Mass/Light Ratio*

As was shown in Sec. VI, the different solutions for the stellar M/L ratios and halo parameters in Tables III–V can vary widely and yet provide nearly equally good fits to the observed rotation curves. A good example is NGC 1085, where the disk M/L ratio varies by a factor 3 among the different solutions, while the rms barely changes. Nevertheless, there are several arguments suggesting that the stellar M/L ratio from the maximum-disk solution is likely to be closest to the correct value. First, as shown in the previous section, the stellar mass derived by the maximum-disk solution is tightly correlated with the galaxy luminosity. The stellar masses derived by the two other solutions show much larger scatter. Second, in most galaxies, the observed shape of the inner rotation curve is well matched by the maximum-disk solutions, and for at least half of all galaxies the matchup extends over the entire observed rotation curve. Third, it will be shown in a future paper that for galaxies with 21 cm rotation curves a full solution for stellar and halo parameters results in a stellar M/L ratio that is close to the maximum-disk solution for most objects. Van Albada *et al.* (1985) present additional arguments why the maximum-disk solution is likely to be closest to being correct. Nevertheless, none of these arguments is very compelling, and one cannot rule out the possibility that dark matter makes a significant contribution to the mass of a galaxy inside an optical radius. However, it cannot have a distribution significantly different from that of the luminous matter.

### *c) Halo Mass and Halo Density*

A rough lower limit to the halo mass inside any radius can be obtained by comparing the stellar mass predicted by the maximum-disk solution with the total mass given by the observed rotation curve. (The difference between the total and stellar masses must be a lower limit to the halo mass, because otherwise the halo would have a hollow center.) For those galaxies with a significant excess of mass in the halo at some standard radius (e.g., the optical edge of the galaxy), the parameters for the halo derived by fixed-$\sigma$ or constant-density solutions might be more reliable, and so they can be used to derive an improved estimate of the halo mass and its density and a revised estimate of the stellar M/L ratio. In this way "typical" halo masses and densities for the entire galaxy sample can be derived.

This has been done as follows. To derive a first-order estimate of the total/stellar mass ratio inside the optical radius, the total mass for each galaxy is taken from Table IV, column (10) and the stellar mass is taken from Table III, column (7). (Remember that the total mass was derived by using the fixed-$\sigma$ solution to extrapolate the observed rotation curve, where necessary, to the optical radius). The constant-density solutions are used to derive the halo density and a revised stellar M/L ratio. (Because the rotation curves have limited sensitivity to the halo component, these solutions, with only one free parameter for the halo, are preferred over the fixed-$\sigma$ solutions).

For all 37 galaxies, the median first-order total/stellar mass ratio is about 1.5. For the 19 galaxies where this ratio exceeds 1.5 (and hence have significant halo components), one might then expect the constant-density solutions to provide meaningful results. The solutions in Table V for these galaxies have a disk M/L ratio that is lower than the maximum-disk solution by an average factor of 1.26. The bulge M/L ratio is not significantly different. Since these galaxies are primarily disk dominated, the total stellar M/L ratio is also a factor of about 1.2 lower. Hence the correct ratio of total/stellar mass is more like 1.8. On this basis, one finds that the stellar and dark matter contribute roughly equal mass inside the optical radius. It should be reiterated that the mass determination is based on an extrapolation of the observed rotation curve to the limits of the optical photometry, which is often at a radius significantly beyond the end of the velocity measurements. This result is consistent with the findings of van Albada *et al.* (1985) and Carignan and Freeman (1985) for galaxies with 21 cm rotation curves.

The halo density $\rho_0$ for the 19 galaxies with a significant halo still shows a wide scatter. However, there is a loose correlation with total mass, as is shown in Fig. 5. The slope of the correlation is roughly $\rho_0 \propto M^{-1}$. While suggestive, this correlation should not be taken very seriously. Carignan and Freeman find halo densities for three dwarf galaxies with masses of $< 10^{10} M_\odot$ to be of order $20 \times 10^{-26}$ g cm$^{-3}$. Including their points here would seriously weaken the correlation.

### *d) Additional Constraints on the Halo Mass*

Since the straightforward model fits do not constrain the halo component very well, it is of interest to look at alternative strategies that might place limits on the halo mass and disk M/L ratio. Three possible ways will be examined here.

#### *1) Disk stability*

One of the major drivers in the search for massive halos is the need to find a mechanism to stabilize the disks of spiral galaxies against bar-like instabilities. Ostriker and Peebles (1973) and Efstathiou, Lake, and Negroponte (1982) have shown that massive, hot halos can do the job, provided the halo mass satisfies certain criteria. Although the two groups of authors give different criteria, they demand essentially that the halo possess a mass as much or more than the disk inside a radius containing most of the disk light.

Recent numerical and theoretical work on the stability of disks shows that these criteria are probably oversimplified

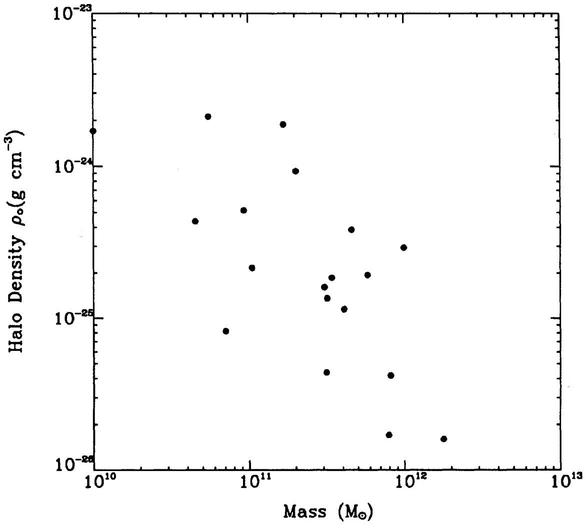

FIG. 5. Correlation of halo density $\rho_0$ with total mass $M$. Only galaxies with significant halo masses are included.

and that ultimately stability depends as much on the details of the mass distribution of a galaxy (centrally concentrated galaxies with an inner Linblad resonance being more stable) and the radial-velocity dispersion of the stellar disk (Sellwood 1983). In fact, one would rather work in the opposite direction and use the rotation curves to estimate the halo mass distribution and then verify that the conditions for stability are satisfied.

#### *2) Physical plausibility*

If the halo is composed of collisionless particles (their exact nature being unimportant here), then one might expect the halo to obey certain "reasonable" conditions. One is that the halo density profile decrease monotonically away from the center. A second is that the halo velocity dispersion also decreases monotonically away from the center. In the idealized case of a spherically symmetric galaxy, the halo will satisfy the equation of hydrostatic equilibrium:

$$\frac{d}{dr}(\rho\sigma_r^2) + \frac{2\beta\rho\sigma_r^2}{r} = -\frac{\rho G m(r)}{r^2} \tag{5}$$

$$= -\frac{\rho v_c^2}{r}.$$

In this equation, $\rho$ is the halo density and $m(r)$ is the total mass inside radius $r$. The anisotropy parameter $\beta = 1 - \sigma_t^2/\sigma_r^2$, where $\sigma_t$ and $\sigma_r$ are the tangential and radial dispersions, respectively. If the velocity distribution is isotropic ($\beta = 0$), the velocity dispersion at any radius is given by

$$\sigma^2(r) = \frac{1}{\rho}\int_r^\infty \frac{\rho(r')Gm(r')}{r'^2}\,dr'.$$

A halo with a density profile given by Eq. (4) could not exist in isolation, since, for an isotropic distribution function, it is easily shown that the velocity dispersion drops in the center by a factor of 1.47 relative to the outside. If anisotropy in the velocity distribution is allowed, then a further constraint is that the anisotropy parameter $\beta$ increases monotonically away from the center. With this constraint it can be shown that the halo of Eq. (4) still cannot exist in isolation since, if $\sigma^2$ is constant, $\beta$ must have a maximum at a finite radius.

A check on the central velocity dispersion for the halo density profiles determined by the fixed-$\sigma$ method shows that for all but two galaxies (UGC 12810 and NGC 3495) the central velocity dispersion is a maximum. In fact, for most halos, the central velocity dispersion is quite a bit higher than the asymptotic value (by factors of 2 and 3), and hence the halos are "isothermal" only at radii where the stellar component is negligible. The halos of the constant-density solutions require even higher central dispersions. Reversing the argument, if the dark matter is indeed isothermal, it must dominate the mass distribution everywhere.

#### *3) Features in rotation-curve profile*

Casertano (1983) has shown how a truncation in the luminosity profile in NGC 5907 can produce a characteristic "break" in the rotation curve. By matching the predicted size of the break with that observed, he is able to estimate the relative disk and halo fractions. Such breaks can be produced by any discontinuity in the disk profile, and inspection of the profiles in Fig. 2 shows that discontinuities are not uncommon. They are usually characteristic of the edges of lens components or bright inner disks with strong spiral structure. A good example is seen in NGC 3067. The corresponding disk rotation curve has a sharp change in slope at the location of the break at 6 kpc.

A casual inspection of the rotation curves in Fig. 2 turns up few cases where a characteristic break in the predicted rotation curve actually matches what is observed. However, both the observed and predicted curves do show features. This lack of matchup may be due to several factors: (i) measurement errors are large; (ii) the measured rotation curve is influenced by noncircular motions; (iii) the measured profiles have been smoothed improperly; (iv) the features in the disk luminosity profiles arise from local variations in the M/L ratio (e.g., due to patches of recent star formation) and are not reflected in the underlying disk mass distribution; (v) the disk mass is truly low and has little contribution to the observed rotation curve. Just which of these features is at work is not immediately clear. In at least one galaxy, NGC 2998, ripples in the predicted rotation curve *are* seen to follow the measured profile closely. At the opposite extreme, a very pronounced feature in the disk profile of UGC 12810 is completely unnoticed in the measured rotation curve. This feature is washed out if the disk M/L ratio is reduced by a factor of 2 and extra halo introduced, so roughly speaking, the lack of a feature in the observed profile might be taken as evidence for a halo contribution to the rotation curve at least comparable to the disk contribution at that radius.

## VIII. BULGE MASSES

From the decompositions and model fits, one derives the total bulge mass and its distribution. An independent check on the bulge dynamics is provided by the velocity dispersion measurements that exist for 15 of these galaxies (Whitmore, McElroy, and Tonry 1985). Since bulges are not isolated systems, one cannot use the virial theorem to estimate the bulge mass directly from the velocity dispersion and luminosity profile. However, from the equation of hydrostatic equilibrium (5), one can derive a variant of the virial theorem for any component embedded within a spherically symmetric system:

$$M_B\langle\sigma^2\rangle = \frac{1}{3}\int_0^\infty \frac{Gm(r)}{r}\,dm_b, \tag{6}$$

where $m(r)$ and $m_b(r)$ are the cumulative total and bulge mass inside radius $r$, respectively, $M_B$ is the total bulge mass, and $\langle\sigma^2\rangle$ is the mean one-dimensional velocity dispersion. This equation does not depend on any assumptions about anisotropy in the bulge velocity distribution.

The bulge and total mass distributions are known directly from the fits to the rotation curves. Hence, Eq. (6) can be used to determine the mean $\langle\sigma^2\rangle$ for the bulge. This has been done for the 15 galaxies with measured dispersions and the results are listed in Table VI. It is not expected that the predicted and measured dispersions will agree, since the predicted value refers to the entire bulge, while the measured value refers to some average of the inner part only with some unknown amount of disk contribution; also, the condition of spherical symmetry is not satisfied. Nevertheless, the measured dispersion exceeds the predicted by only a factor 1.2 with a scatter of about 30%. It is also interesting to note that the halo dispersion $\sigma_H$ from the fixed-$\sigma$ method is a factor 1.4 larger than the measured bulge dispersion $\sigma_{\rm obs}$ and 1.7 larger than the predicted dispersion $\sigma_{\rm pred}$. For comparison, for a bulge with an $r^{-3}$ density profile embedded in a singular isothermal sphere potential, this ratio would be only $(3/2)^{1/2}$ or 1.2.

TABLE VI. Bulge dynamics.

| Name | $\sigma_{pred}$ | $\sigma_{obs}$ |
|---|---|---|
| N753 | 91 | 103 |
| N801 | 105 | 136 |
| N1353 | 94 | 84 |
| N1417 | 118 | 134 |
| N1620 | 86 | 116 |
| N2998 | 63 | 79 |
| N3200 | 127 | 165: |
| N4062 | 49 | 97 |
| N4448 | 90 | 176 |
| N7217 | 146 | 132 |
| N7537 | 61 | 118 |
| N7541 | 92 | 67 |
| N7606 | 126 | 160 |
| N7664 | 74 | 103 |
| U11810 | 62 | 60 |

The reasonable agreement between $\sigma_{\rm pred}$ and $\sigma_{\rm obs}$ is not direct evidence that the estimated $(M/L)_{\rm B}$ is correct, since $\sigma_{\rm pred}$ depends directly on the rotation curve and bulge luminosity profile and only indirectly on $(M/L)_{\rm B}$ insofar as the fits to the observed profile are correct. Hence the agreement of the dispersions is a check more on the entire bulge/disk decomposition and rotation-curve fitting process and not just the $(M/L)_{\rm B}$ alone.

## IX. CONCLUSIONS

The primary conclusion is that optical rotation curves do not always place strong constraints on the amount of dark matter in galaxies. In most galaxies, the rotation curve that one computes from the luminosity profile assuming a constant M/L ratio provides a good match to the observed curve out to a radius where the predicted curve turns over. Most optical rotation curves do not extend much past this peak. This conclusion has already been anticipated by Van Albada *et al.* (1985).

Various methods have been tried to estimate the halo mass and distribution. The simplest way is to estimate the maximum M/L ratio for the bulge and disk components consistent with the observed rotation curve and then attribute any excess in the observed rotation curve at large radii to a dark halo. By doing this and then correcting the stellar M/L ratio to produce a physically more plausible halo, it is estimated that stars and dark matter contribute roughly equal amounts inside the optical edge of a galaxy.

The stellar M/L ratio is shown to correlate with galaxy mass, morphological type, and inclination. The light distribution correlates well with the mass distribution insofar as the shape of the rotation curves agrees well with the observed rotation curve (with a few notable exceptions). The observed bulge dynamics (i.e., velocity dispersions) agree reasonably well with what one would predict based on the rotation curves and the bulge/disk luminosity profile decompositions.

Although most galaxies show some evidence for the presence of a dark halo, several galaxies have rotation curves that can be reproduced by assuming a constant M/L ratio for the luminosity distribution and *no* halo. This result is the same found by Kalnajs (1983), and leaves open the possibility that some galaxies may not possess massive halos. It would be of great interest to extend the rotation curves of these objects and see if they remain flat. H I observations with the VLA would probably be required.

Implicit in all this work is the assumption that the stellar M/L ratio is constant within a galaxy. While color gradients are usually small, it would be useful to map the light distribution in an infrared band which is expected to provide a better measure of the underlying mass distribution (as well as minimize problems with internal extinction).

I wish to thank M. Geller, J. Huchra, and R. Schild for critical comments on the manuscript, and R. Sancisi for illuminating discussions. This work was partially supported by NSF Grant No. AST-84-51724.

## REFERENCES

Boroson, T. (1981). Astrophys. J. Suppl. **46**, 177.

Bosma, A. (1981). Astron. J. **86**, 1791.

Bosma, A., and van der Kruit, P. C. (1979). Astron. Astrophys. **79**, 281.

Burstein, D. (1985). Private communication.

Burstein, D., Rubin, V. C., Thonnard, N., and Ford, W. K. (1982). Astrophys. J. **253**, 70.

Carignan, C., and Freeman, K. C. (1985). Astrophys. J. **294**, 494.

Casertano, S. (1983). Mon. Not. R. Astron. Soc. **203**, 735.

de Vaucouleurs, G. (1948). Ann. Astrophys. **11**, 247.

de Vaucouleurs, G., de Vaucouleurs, A., and Corwin, H. G. (1976). *Second Reference Catalog of Bright Galaxies* (University of Texas, Austin) (RC2).

Efstathiou, G., Lake, G., and Negroponte, J. (1982). Mon. Not. R. Astron. Soc. **199**, 1069.

Elmegreen, B. G., and Elmegreen, D. M. (1985). Astrophys. J. **288**, 438.

Elmegreen, D. M., and Elmegreen, B. G. (1984). Astrophys. J. Suppl. **54**, 127.

Faber, S. M. (1982). *Astrophysical Cosmology*, edited by H. A. Bruck, G. V. Coyne, and M. S. Longair (Pontifica Academia Scientarum, Vatican City), p. 191.

Faber, S. M., and Gallagher, J. S. (1979). Annu. Rev. Astron. Astrophys. **17**, 135.

Goad, J. W. (1976). Astrophys. J. Suppl. **32**, 89.

Kalnajs, A. (1983). In *Internal Kinematics and Dynamics of Disk Galaxies*, IAU Symposium No. 100, edited by E. Athanassoula (Reidel, Dordrecht), p. 87.

Kent, S. M. (1983). Astrophys. J. **266**, 562.

Kent, S. M. (1984). Astrophys. J. Suppl. **56**, 105.

Kent, S. M. (1985). Publ. Astron. Soc. Pac. **97**, 165.

Ostriker, J. P., and Peebles, P. J. E. (1973). Astrophys. J. **186**, 467.

Rubin, V. C., Burstein, D., Ford, W. K., and Thonnard, N. (1985). Astrophys. J. **289**, 81.

Rubin, V. C., Ford, W. K., and Thonnard, N. (1980). Astrophys. J. **238**, 471.

Rubin, V. C., Ford, W. K., Thonnard, N., and Burstein, D. (1982). Astrophys. J. **261**, 439.

Schild, R., and Kent, S. (1981). Proc. S.P.I.E. **290**, 186.

Sellwood, J. A. (1983). In *Internal Kinematics and Dynamics of Disk Galaxies*, IAU Symposium No. 100, edited by E. Athanassoula (Reidel, Dordrecht), p. 197.

Thuan, T. X., and Gunn, J. E. (1976). Publ. Astron. Soc. Pac. **88**, 543.
Toomre, A. (1963). Astrophys. J. **138**, 385.
Tully, R. B., Mould, J. R., and Aaronson, M. (1982). Astrophys. J. **257**, 527.
van Albada, T. S., Bahcall, J. N., Begeman, K., and Sancisi, R. (1985). Astrophys. J. **295**, 305.
Wevers, B. M. H. (1984). Ph. D. thesis, Groningen University.
White, S. D. M., and Rees, M. J. (1978). Mon. Not. R. Astron. Soc. **183**, 341.
Whitmore, B. C., Mc Elroy, D. B., and Tonry, J. L. (1985). Astrophys. J. Suppl. **59**, 1.